JULY 1967
REPORT SM-49105-F1

STRESS CORROSION CRACKING OF TITANIUM ALLOYS AT AMBIENT TEMPERATURE IN AQUEOUS SOLUTIONS

GPO PRICE $ _____

CFSTI PRICE(S) $ _____

Hard copy (HC) ___3.00___

Microfiche (MF) ___.65___

ff 653 July 65

YEARLY SUMMARY REPORT
JULY 1966 THROUGH JUNE 1967
UNDER CONTRACT NAS 7-488

ASTROPOWER LABORATORY
2121 CAMPUS DRIVE · NEWPORT BEACH, CALIFORNIA

MISSILE & SPACE SYSTEMS DIVISION
DOUGLAS AIRCRAFT COMPANY, INC.
SANTA MONICA/CALIFORNIA

N68-12544
(ACCESSION NUMBER)   (THRU)
87   1
(PAGES)   (CODE)
CR-91165   17
(NASA CR OR TMX OR AD NUMBER)   (CATEGORY)

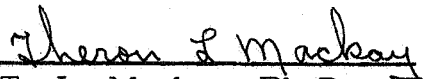FF No. 602(C)

DOUGLAS

Report SM-49105-F1

STRESS CORROSION CRACKING OF TITANIUM ALLOYS AT AMBIENT TEMPERATURE IN AQUEOUS SOLUTIONS
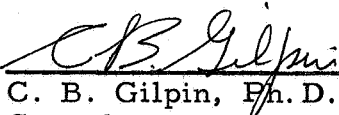
Yearly Summary Report
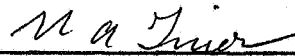July 1966 Through June 1967

Contract NAS 7-488

Administered by
Chief, Research SRT NASA Headquarters
Code RRM

Prepared by:

T. L. Mackay, Ph. D.
Senior Research Scientist

C. B. Gilpin, Ph. D.
Consultant

Approved by:

N. A. Tiner, Ph. D.
Head, Materials Department

MISSILE & SPACE SYSTEMS DIVISION
ASTROPOWER LABORATORY
Douglas Aircraft Company
Newport Beach, California

FOREWORD

This report was prepared by Astropower Laboratory, Douglas Aircraft Company, under NASA contract NAS 7-488. It is a yearly summary report and covers work conducted from July 1966 through June 1967. The work is administered by the Chief, Research SRT NASA Headquarters, Code RRM, with Mr. W. Raring as Project Scientist.

This report was jointly authored by Drs. T. L. Mackay, C. B. Gilpin and N. A. Tiner. Messrs. R. G. Ingersoll, W. A. Cannon, S. M. Toy and Dr. S. K. Asunmaa have greatly contributed to the performance of this work.

ABSTRACT

Stress corrosion tests in distilled and aqueous salt solutions were made at ambient temperature employing single edge notch specimens of titanium Ti-5Al-2.5Sn, Ti-8Al-1Mo-1V, Ti-6Al-4V, and Ti-13V-11Cr-3Al alloys. The all-beta alloy (Ti-13V-11Cr-3Al) showed no appreciable susceptibility to stress corrosion cracking while alpha-beta and near-alpha alloys (Ti-8Al-1Mo-1V and Ti-5Al-2.5Sn) did exhibit SCC. Electron microfractographs of the stress corrosion fractures of alpha-beta and near-alpha alloys showed a mixture of cleavage and ductile dimple rupture. Cleavage areas were larger in salt solution tests. Profiles of the fractured surfaces of Ti-5Al-2.5Sn and Ti-6Al-4V showed that cleavage occurred in the alpha phase and at the alpha-beta phase boundaries.

Electron microautoradiography studies of the distribution of hydrogen by gas adsorption in titanium alloys showed — (1) a uniform distribution in Ti-13V-11Cr-3Al alloy, (2) a concentration of hydrogen in beta phase of Ti-8Al-1Mo-1V and Ti-6Al-4V alloys, and (3) a segregation of hydrogen at beta-precipitates in alpha grain boundaries in Ti-5Al-2.5Sn. The concentration of hydrogen in the beta phase of Ti-6Al-4V with 40 ppm hydrogen was estimated to be 285, and that in the beta phase of Ti-8Al-1Mo-1V and Ti-5Al-2.5Sn was 450 ppm. It is believed that the higher concentration of hydrogen in beta phase of Ti-5Al-2.5Sn and Ti-8Al-1Mo-1V contributes to the stress corrosion susceptibility of these alloys.

Potentiostat curves for Ti-5Al-2.5Sn and Ti-6Al-4V in 3% NaCl, pH 6.5, were determined. Oxygenation was observed to shift the cathodic polarization curves in an electropositive direction, but did not greatly affect the anodic curves. Stressing the specimens did not affect the cathodic polarization. Some electrochemical changes occurred in the anodic branch which appeared to be dependent on the hydrogen content of the material.

CONTENTS

FIGURES

1.0 INTRODUCTION

The stress corrosion cracking of titanium and its alloys in salt environments at elevated temperatures of approximately 500 to 800°F has received much attention in experimental studies.[1-3] Until recently, it was believed that titanium alloys were completely resistant to stress corrosion cracking in aqueous salt environments at room temperature. Brown[4] developed a new test, which employed a specimen with a notch that had been sharpened by fatigue for studying stress corrosion cracking of high strength steels. When this test was applied to titanium alloy specimens, it was discovered that the fracture strength was reduced in a 3.5% NaCl environment, in tap water, and in distilled water.[5] A considerable amount of testing has been performed during the past two years to develop new titanium alloys and heat treating methods to prevent this susceptibility to stress corrosion.

In addition to the reduction of fracture toughness observed with notched specimens, the effect of an aqueous environment has shown up in other studies. Judy et al.[6] have shown that the low cycle fatigue crack propagation of Ti-7Al-2Cb-1Ta is greater in aqueous environments at all strain ranges than in air. The reaction to 3.5% NaCl is more severe than to distilled water.

Studies have been made to relate stress corrosion susceptibility to composition. Reactive Metals Inc.[7] have shown for the Ti-xAl-2Cb-1Ta and Ti-xAl-3Cb alloy that increasing aluminum from 6 to 7% increases susceptibility; whereas, adding molybdenum to both Ti-7Al-2Cb-1Ta and Ti-7Al-3Cb alloys decreases susceptibility. Lane et al.[8] suggested that the stress corrosion of titanium alloys is related to the ordering observed in the 6 to 10% aluminum range when heat treated from 900°F to 1300°F. The presence of the beta stabilizers, Mo, V and Cb, decreased sensitivity.

Attempts have also been made to relate microstructure to the degree of susceptibility to stress corrosion in aqueous salt solutions. Hatch et al.[9] has shown that the typical Ti-8Al-1Mo-1V microstructure which exhibits a continuous alpha matrix is very susceptible; however, by heat treating the same alloy to produce a discontinuous alpha in a beta matrix, the stress corrosion susceptibility was reduced. Lane et al.[8] observed an apparent correlation between susceptibility and microstructure for a great number of alloys.

Microstructures with coarse and long matrix platelets were susceptible; whereas materials with fine platelets and alpha island dispersions were not susceptible. Beck[10] found a large change in fracture strength of Ti-8Al-1Mo-1V in aqueous KCl solution with solution treatment between $900^{\circ}C$ and $1000^{\circ}C$. Erbin[11] showed that Ti-6Al-4V processed above the beta transus and rapidly quenched to produce martensitic acicular structure had less stress corrosion susceptibility than the alpha-beta structure produced by working in the alpha-beta region.

Lane et al.[8] found that fractures did not follow any definite metallographic path such as prior beta grain boundaries. Fracture was transgranular through alpha and alpha-beta alloys. Hatch et al.[9] found that fracture is a low energy failure, and is accompanied by very little deformation. There was very little slip or twinning adjacent to the crack. Electron fractographic studies of the fracture have added a great deal to our knowledge about the mode of failure for titanium alloys. Hatch et al.[9] found that the fracture propagates by a combination of quasi-cleavage and ductile rupture. Judy et al.[6] conducted fractographic studies on low cycle fatigue in different environments. For the Ti-7Al-2Cb-1Ta alloy tested in distilled water, there was a mixture of quasi-cleavage and fatigue striations. For specimens tested in 3.5% NaCl, the major portion of the fractured surface showed quasi-cleavage. Thus the amount of quasi-cleavage was directly related to the rate of crack growth. Fractographic studies have clearly demonstrated that in notched stress corrosion tests above the threshold stress, failure always occurred in a few minutes by quasi-cleavage; whereas below the threshold, failure was of the ductile dimpled rupture type.

Electrochemical mechanism studies of stress corrosion of titanium alloys in aqueous salt solutions are underway at several laboratories. Feige and Murphy[12] have shown that titanium alloys which can be pitted with anodic potentials of less than 20 volts are susceptible to stress corrosion failure. Specimens are not protected by anodic potential, but are protected by about 1000 mv vs. SCE of cathodic potential. They interpret these results and others in terms of film rupture models, and propose the following mechanisms in stress corrosion cracking:

1. Film rupture at the surface due to applied load.
2. Cl^-, Br^- and I^- will not passivate this area, whereas OH^- or $O^=$ will.
3. H^+ will be discharged at the cathode which is the surface protective film.
4. Dissolution of titanium takes place.
5. The rate of reaction is dependent upon the rate of slip and the rate of passivation.

The objectives of the present studies were to determine the micro-processes in stress corrosion failure of different titanium alloys at ambient temperature in aqueous salt solutions using the experimental techniques already developed by Astropower Laboratory. These techniques included (1) examination of stress corrosion cracked surfaces by microfractography, (2) determination of the hydrogen distribution in the microstructure by electron microautoradiography, and (3) evaluation of possible electrochemical reactions by potentiostatic measurements. The results and investigations are presented in this report.

2.0 EXPERIMENTAL EVALUATIONS

2.1 Alloy Selection

The following titanium alloys were selected[13] for detailed investigation of the mechanism of stress corrosion cracking:

1. Ti-5Al-2.5Sn (an alpha alloy)
2. Ti-6Al-4V (an alpha-beta alloy)
3. Ti-8Al-1Mo-1V (a super alpha alloy)
4. Ti-13V-11Cr-3Al (a beta alloy)

Hatch et al[9] studied the mechanical conditions necessary for failure and found that susceptibility is related to the thickness of the test specimen. For Ti-8Al-1Mo-1V alloy, a 0.45 inch sheet is highly susceptible, whereas a 0.25 inch sheet is not. For Ti-6Al-4V in the mill annealed condition, the thickness must be greater than 0.045 inch for susceptibility. Feige and Murphy[14] have reported minimum thickness of 0.025 inch for Ti-8Al-1Mo-1V and 0.045 inch for Ti-6Al-4V. Hatch et al[9] further showed a fatigue crack, from which a plain strain failure initially propagates, is an essential condition. Cracks put in by shear failure did not propagate. These results suggest that the effect of thickness is related to a plain strain condition.

Sheet materials of Ti-5Al-2.5Sn, Ti-6Al-4V and Ti-8Al-1Mo-1V were obtained from Titanium Metals Corporation; the thickness of Ti-5Al-2.5Sn and Ti-6Al-4V was 0.075 inch, while the thickness of the Ti-8Al-1Mo-1V alloy was 0.109 inch. A sheet of Ti-13V-11Cr-3Al alloy, 0.075 inch in thickness, was obtained from Crucible Steel Company. A sheet of Ti-8Al-1Mo-1V, 0.045 in thickness, with a heat treatment described by Hatch et al[9] to produce a discontinuous alpha in a beta matrix, was obtained from Titanium Metals Corp. The chemical composition of the selected alloys is shown in Table I. The heat treatment for each alloy is shown in Table II with mechanical properties.

The microstructure of each alloy is shown in Figures 1a, 1b, 1c and 1d. Only the beta alloy, Ti-13V-11Cr-3Al, showed a coarse grain structure. The microstructure of the two alpha-beta alloys, Ti-8Al-1Mo-1V and Ti-6Al-4V, exhibited a continuous alpha matrix.

TABLE I

COMPOSITION OF TITANIUM ALLOYS

	Al	Sn	Mo	V	Fe	Cr	C	O	N	H
5Al-2.5Sn	5.0	2.4			0.27		0.25	0.10	0.015	0.007
6Al-4V	5.8			3.9	0.12		0.023	0.13	0.019	0.004
13V-11Cr-3Al	3.5			13.6	0.22	10.2	0.04		0.03	0.0154
8Al-1Mo-1V	7.8		0.91	0.94	0.20			0.067		0.0036
8Al-1Mo-1V	7.7		0.95	0.85	0.21			0.088		0.0071

(Titanium Metals
Heat Treatment 2B2)

TABLE II

MECHANICAL PROPERTIES OF TITANIUM ALLOYS
FOLLOWING HEAT TREATMENTS

Alloy	Heat Treatment	0.2% Yield Ksi	Ultimate Tensile Ksi	El %
Ti-5Al-2.5Sn	Mill Anneal	130.1	141.9	15.5
Ti-6Al-4V	Mill Anneal	138.0	144.5	13.0
Ti-8Al-1Mo-1V	Duplex Anneal	144.1	152.7	21.5
Ti-13V-11Cr-3Al	Mill Anneal	140.4	143.2	23.4
Ti-8-1-1	Titanium Metals Heat Treatment Process 2B2 Heat G-1618	127.4	142.0	15.0
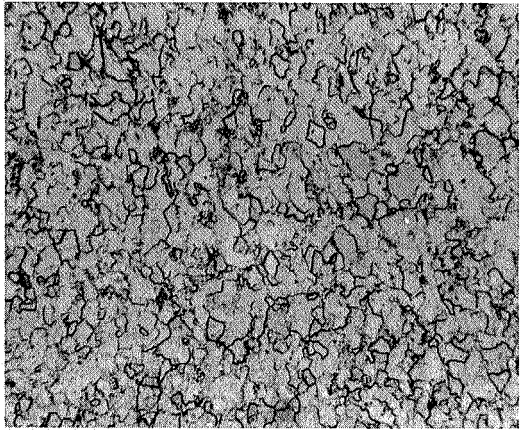
(a)
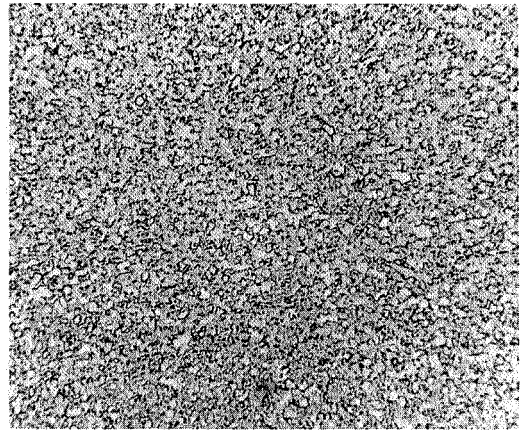
(b)
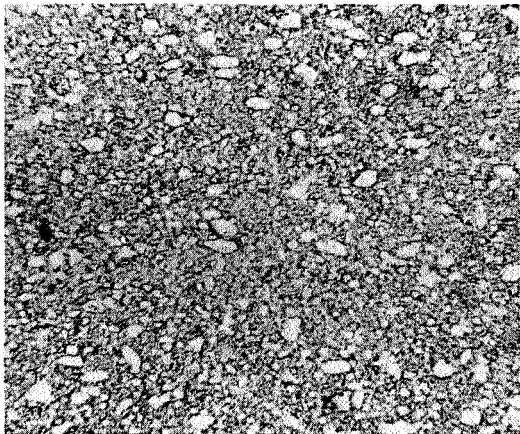
(c)
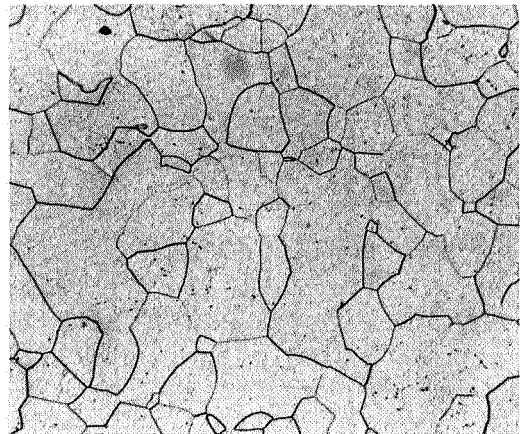
(d)

a. Ti-5Al-2.5Sn
b. Ti-6Al-4V
c. Ti-8Al-1Mo-1V
d. Ti-13V-11Cr-3Al

C2590

Figure 1. Microstructure of Titanium Alloys, Mag. 200X

2.2 Specimen Configuration

The process of stress corrosion cracking in alloys usually commences as a pitting attack rather than a uniform corrosion, and in the general case, stress corrosion does not initiate until a pit grows deep enough to act as a stress raiser. By inserting a fatigue crack in the specimen before commencing the test, stress corrosion can be caused to initiate immediately upon application of stress. The purpose of the experimental studies conducted during this contract was to evaluate the metallurgical conditions around the crack tip leading to stress corrosion failure. For this reason, it was desirable to select a specimen configuration for which the stress conditions at the crack tip were well understood.

During the past few years a considerable amount of work has been done to evaluate the stress intensity factor, K, in fracture toughness testing. It has been found that the stress intensity factor at the point of crack instability, K_c, is dependent on the specimen configuration. However, the plane strain fracture toughness value, K_{Ic}, is independent of any specimen dimension and thus provides a material characteristic. From this work, several specimen types suitable for K_{Ic} measurements have evolved. The specimens have been studied in great detail and the elastic stress conditions around the crack tip are well understood. The yield conditions around the crack tip are also pretty well understood for these specimens. [15]

In this program, the single edge notch specimen was chosen. This specimen is well suited to stress corrosion studies. Furthermore, its size is smaller than other specimen types which allows one to keep the total load applied to a minimum. Figures 2 and 3 show the actual specimen configuration for each of the alloys tested.

In order to assure a plane strain distribution, the specimen must be greater in size than some specified minimum. This minimum is usually given in terms of the thickness B. At the start of the program, the generally accepted minimum was $B \geq 0.65 \left(\dfrac{K_{Ic}}{\sigma_{ys}} \right)^2$. [16] During the time of this investigation, new minimums, based on experimental results, were proposed to the
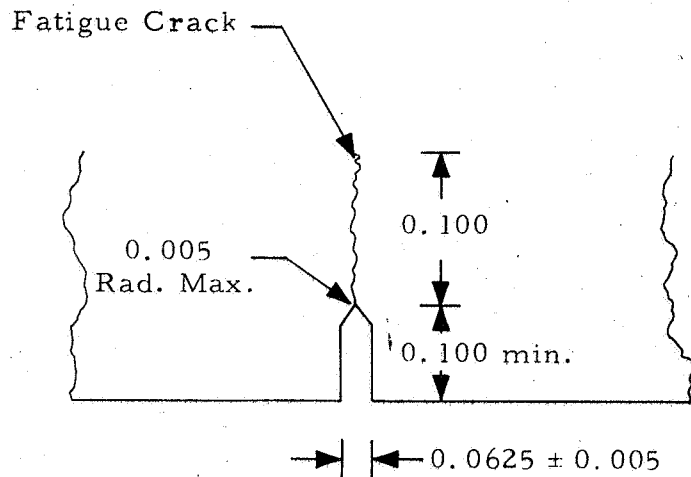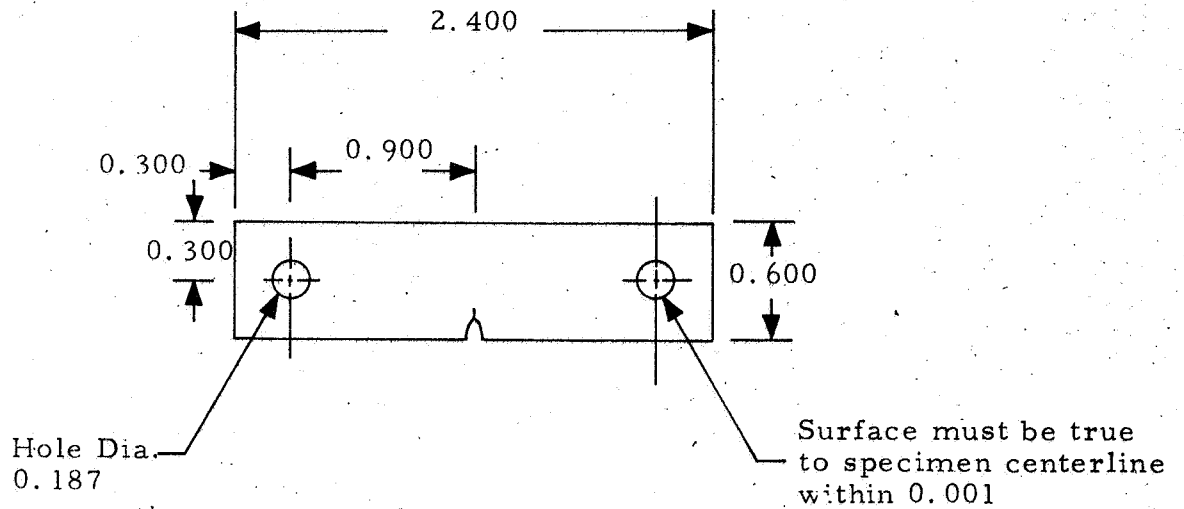
Figure 2. Stress Corrosion Specimen Configuration For 0.075 in.
Thick Titanium Alloys Ti-5Al-2.5Sn, Ti-6Al-4V, and
Ti-13V-11Cr-3Al
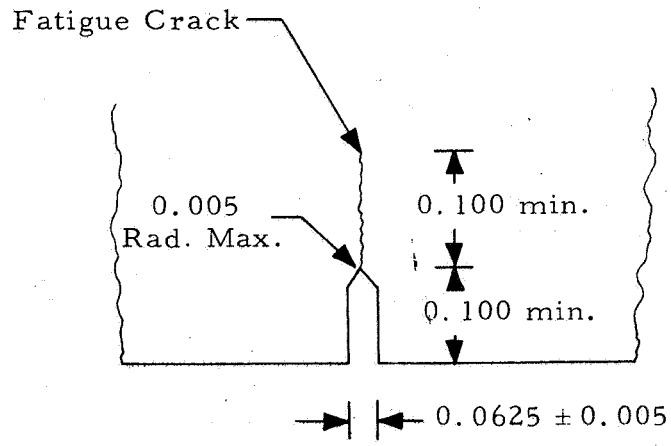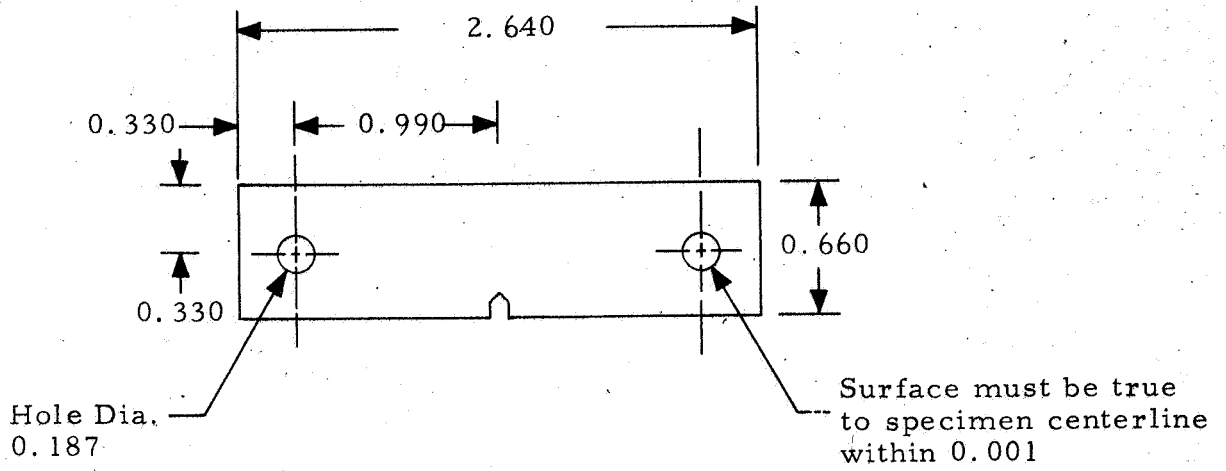
Figure 3. Stress Corrosion Specimen Configuration For
0.109 in. Thick Titanium Alloy, Ti-8Al-1Mo-1V

ASTM Committee E-24 on Fracture Testing of Metals by Brown & Strawley.[17]
This minimum was $B \geq 2.5 \left(\dfrac{K_{Ic}}{\sigma_{ys}} \right)^2$.

Table III shows some typical minimum thicknesses that might be expected for titanium alloys.[18]

On the basis of the $B = 0.65 \left(\dfrac{K_{Ic}}{\sigma_{ys}} \right)^2$ minimums, sheets of Ti-6Al-4V and Ti-13V-11Cr-3Al of thickness 0.075", and sheets of Ti-8Al-1Mo-1V of thickness 0.109" were chosen. Ti-5Al-2.5Sn sheet of 0.075" was also chosen even though it was recognized that plane stress conditions were not met. Plates of 0.525" are too large to test in available apparatus.

In the course of the investigation, it was observed that many of the specimens did not fail in air under plane strain. This can be easily understood in terms of the new thickness minimums also listed in Table III. According to these experiments, the only material studied that should fail in plane strain in air was the Ti-13V-11Cr-3Al alloy.

2.3 Stress Corrosion Cracking Tests

Stress corrosion tests were conducted by loading the single-edge-notched specimen in a Dillon tensile machine shown in Figure 4. The load was measured with a Baldwin-Lima-Hamilton SR-4 Load Cell which is capable of measuring the total load within four pounds. The corrosion solution is contained in a lucite box sealed to the specimen with an epoxy to prevent leakage. Distilled water and 3% NaCl solution at ambient temperature were the corrosion solutions used in the program. Crack extension was observed with a stereo-microscope.

The initial specimen for each alloy was statically loaded and held for five minutes. If the crack did not propagate, the load was increased and again held for five minutes. Eventually a load was reached that caused the specimen to fracture. The time to fracture was measured with a stop watch. The stress intensity factor at crack instability, K_c, was calculated using the load that caused crack propagation to start. For the single-edge-notched specimen, the stress intensity factor, K, has been calculated from the expressions initially recommended by Strawley & Brown.[19]

TABLE III

CALCULATED THICKNESSES FOR PLAIN STRAIN FOR
Ti-6Al-4V, Ti-13V-11Cr-3Al AND Ti-5Al-2.5Sn

Alloy	σ_{ys} ksi	K_{I_c} ksi $\sqrt{in}$	$\left(\dfrac{K_{I_c}}{\sigma_{ys}}\right)^2$	$B = 0.65\left(\dfrac{K_{I_c}}{\sigma_{ys}}\right)^2$	$B = 2.5\left(\dfrac{K_{I_c}}{\sigma_{ys}}\right)^2$
Ti-6Al-4V	135	58	0.185	0.12	0.47
	148	52.2	0.122	0.079	0.31
	152	44.6	0.086	0.056	0.22
	168	38.9	0.054	0.035	0.13
Ti-13V-11Cr-3Al (Avg. of 5 Specimens)	168.3	29.5	0.031	0.020	0.072
Ti-5Al-2.5Sn	117	110	0.808	0.525	2.02
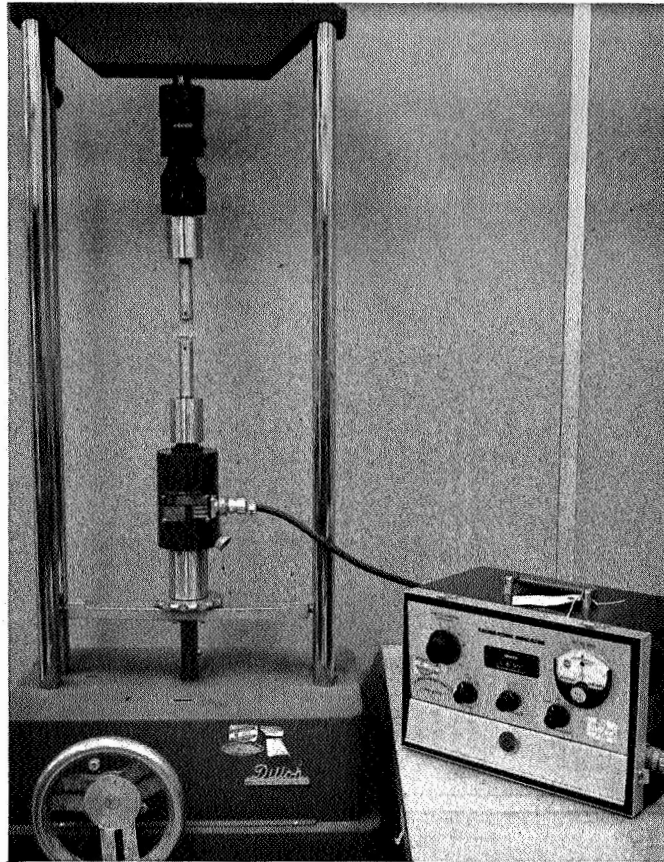
c2591

Figure 4. Stress Corrosion Apparatus

$$K^2 = \frac{P^2}{B^2 w(1-\upsilon^2)}\left[7.59\frac{a}{w} - 32\left(\frac{a}{w}\right)^2 + 117\left(\frac{a}{w}\right)^3\right] \tag{1}$$

P = load
B = thickness
a = crack length
w = width
υ = Poisson's ratio

This equation was determined by experimental compliance measurements. These authors now recommend the equation[17]

$$K = \frac{Pa^{1/2}}{Bw}\left[1.99 - 0.41\frac{a}{w} + 18.70\left(\frac{a}{w}\right)^2 - 38.48\left(\frac{a}{w}\right)^3 + 58.85\left(\frac{a}{w}\right)^4\right] \tag{2}$$

Both equations give the same K value for a/w ratios used in the present investigation.

For each specimen, the initial crack length, a, was measured with a low power microscope following fracture of the specimen, and was used to calculate K_c. Figure 5 shows a typical fatigue crack.

From the results obtained with the initial specimen, load levels were selected for stressing each alloy. The stress intensity factor, K_c, to propagate a crack in air, in a 3% salt solution and in distilled water for the titanium alloy tested, is summarized in Table IV.

Included in this table are a few specimens which were vacuum annealed (10^{-6} torr) at 1400°F for 24 hours and 42 hours to remove the residual hydrogen. A hydrogen chemical analysis for 24 hour vacuum anneal showed 39 ppm, and for 42 hour vacuum anneal showed 30 ppm. A hydrogen chemical analysis of as-received Ti-5Al-2.5Sn showed 61 ppm hydrogen.

This value, K_c, was then plotted versus the time for fracture in Figures 6, 7, 8, and 9. An examination of the graphs shows that there was a minimum value of K_c below which no stress corrosion failure is observed. This is designated K_{ISCC} after Brown.[20]

The reduction of stress intensity factor, K_c, by 3% salt solution at ambient temperature when compared with values obtained in argon or air,
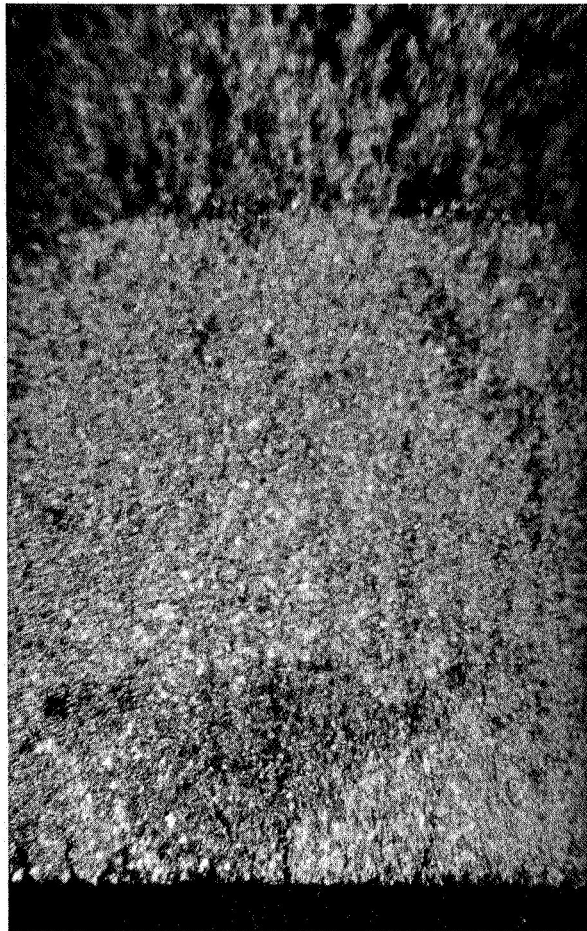
←————— Plane Strain Fracture

←————— End of Fatigue Fracture

←————— Fatigue Fracture

←————— Start of Fatigue Fracture

cz592

Figure 5.   Fracture Surface of Ti-8Al-1Mo-1V.   Mag. 40X.

TABLE IV

STRESS INTENSITY FACTOR, K_c, FOR Ti-8Al-1Mo-1V, Ti-6Al-4V, Ti-13V-11Cr-3Al AND Ti-5Al-2.5Sn IN 3% SALT SOLUTION AND DISTILLED WATER

Alloy	Environment	K_c (Ksi $\sqrt{\text{in}}$)	Time to Fracture (min.)
Ti-8Al-1Mo-1V	Argon	43.7	—
"	Argon	44.8	—
"	3% Salt	28.0	0.6
"	3% Salt	25.2	1.0
"	3% Salt	23.0	1.0
"	3% Salt	18.5	1.5
"	Distilled Water	36.6	1.1
"	Distilled Water	30.4	2.2
"	Distilled Water	24.0	4.0
"	Distilled Water	22.0	6.0
Ti-5Al-2.5Sn	Air	129.0	2.5
"	3% Salt	58.0	2.0
"	3% Salt	48.3	1.0
"	3% Salt	33.0	2.5
"	3% Salt	40.0	1.2
"	3% Salt	34.3	2.5
"	3% Salt	33.0	2.5
"	Distilled Water	95.0	4.6
"	Distilled Water	82.5	3.0
"	Distilled Water	81.0	4.0
"	Distilled Water	71.0	4.0
"	Distilled Water	68.5	4.7
"	Distilled Water	64.0	6.0
Ti-5Al-2.5Sn (Vacuum Heat Treatment 24 hr)	Air	120.0	—
	3% Salt	27.0	—
" 42 hr	Air	120.0	—
" 42 hr	3% Salt	30.0	2.5
Ti-6Al-4V	Air	75.5	—
"	Air	75.5	—
"	3% Salt	57.0	0.5
"	3% Salt	48.0	2.0
"	3% Salt	45.0	2.0
"	3% Salt	44.0	2.0
"	3% Salt	43.0	3.0

(Continued)

TABLE IV (CONTINUED)

STRESS INTENSITY FACTOR, K_c, FOR Ti-8Al-1Mo-1V, Ti-6Al-4V, Ti-13V-11Cr-3Al AND Ti-5Al-2.5Sn IN 3% SALT SOLUTION AND DISTILLED WATER

Alloy	Environment	K_c (Ksi $\sqrt{in}$)	Time to Fracture (min.)
Ti-6Al-4V	3% Salt	42.0	3.0
"	Distilled Water	75.0	2.0
"	Distilled Water	71.5	8.0
"	Distilled Water	71.5	2.7
"	Distilled Water	71.0	8.0
"	Distilled Water	68.5	3.5
"	Distilled Water	68.6	2.2
Ti-13V-11Cr-3Al	Air	101.0	—
"	3% Salt	95.2	0.34
"	3% Salt	90.2	1.0
"	3% Salt	85.2	4.0
"	3% Salt	81.6	55 sec.
"	3% Salt	80.0	5.0
"	3% Salt	73.0	2.0
"	3% Salt	68.5	2.0
"	Distilled Water	97.4	6.0
"	Distilled Water	92.0	16.0
"	Distilled Water	95.0	2.0
"	Distilled Water	90.0	4.0
"	Distilled Water	87.3	7.0
"	Distilled Water	81.2	14.0
"	Distilled Water	83.3	14.0
Ti-8Al-1Mo-1V	Air	62.2	—
(Titanium Metals	Air	62.0	—
Heat Treat Process	3% Salt	54.4	0.2
2B2)	3% Salt	56.8	5.0
"	3% Salt	59.5	0.5
"	3% Salt	56.0	4.0
"	3% Salt	53.0	3.0

Figure 6. Effect of Initial Stress Intensity on Time-To-Fracture for Ti-5Al-2.5Sn at Ambient Temperature

Figure 7. Effect of Initial Stress Intensity on Time-to-Fracture for Ti-8Al-1Mo-1Ti at Ambient Temperature

19

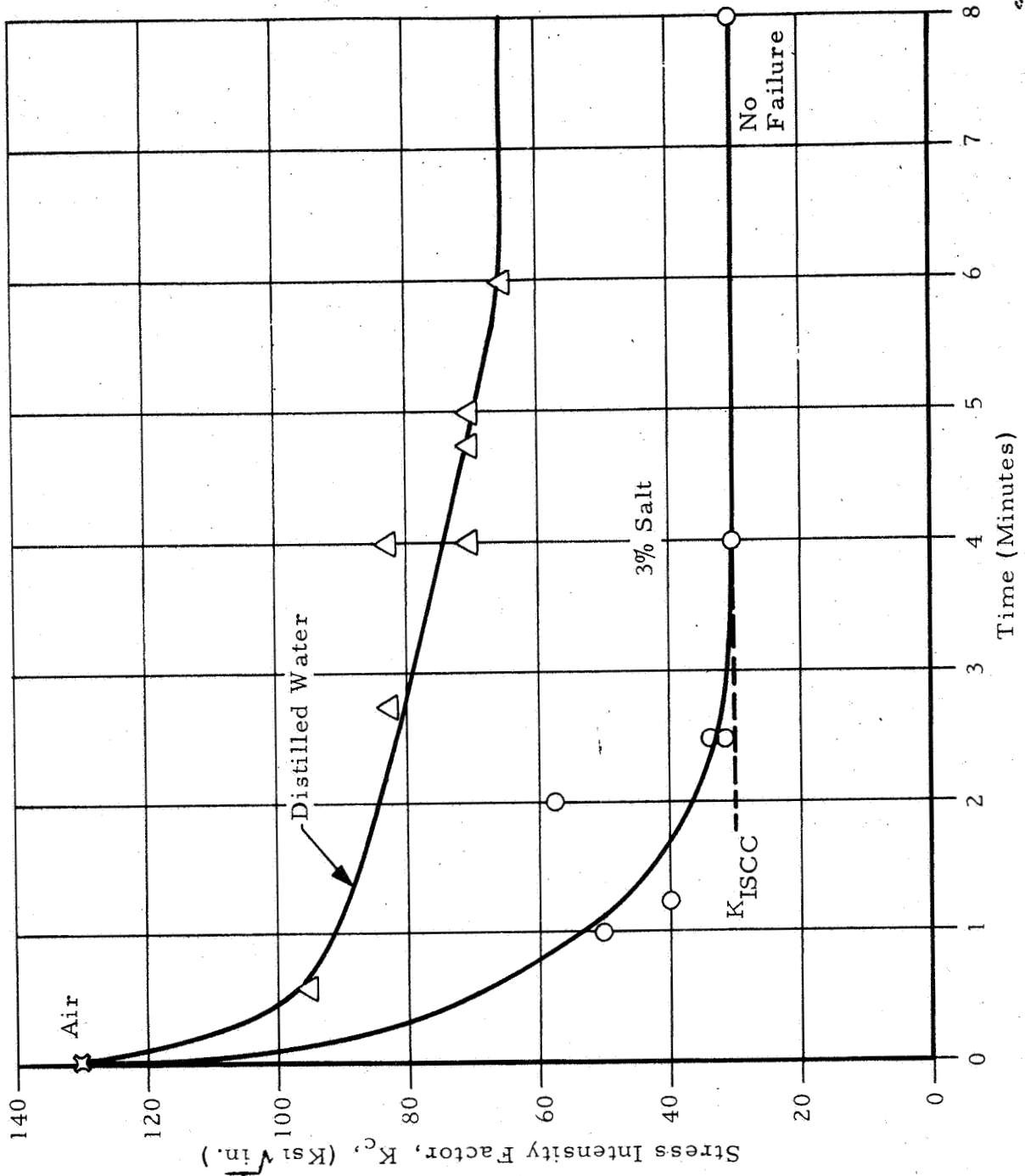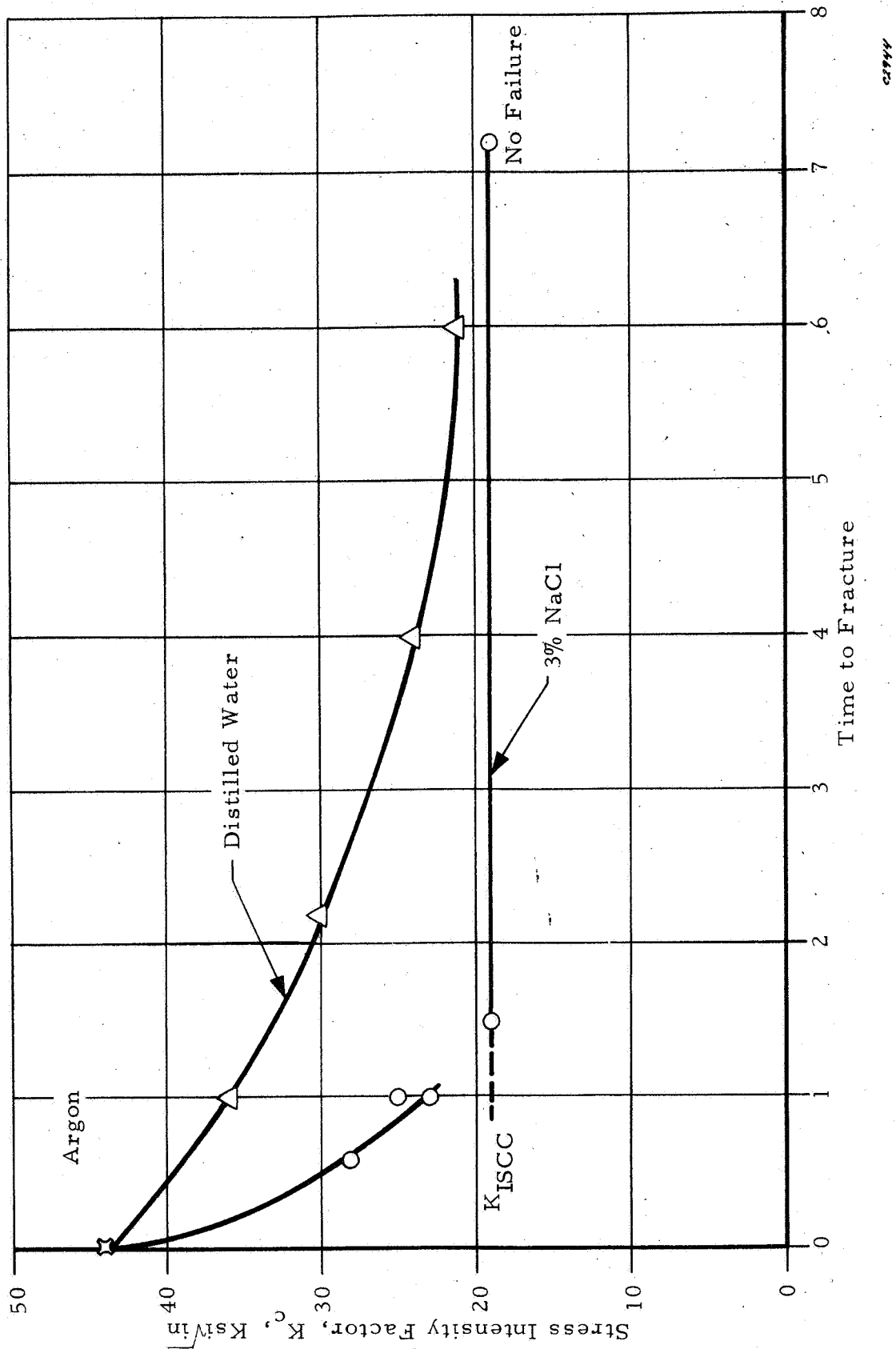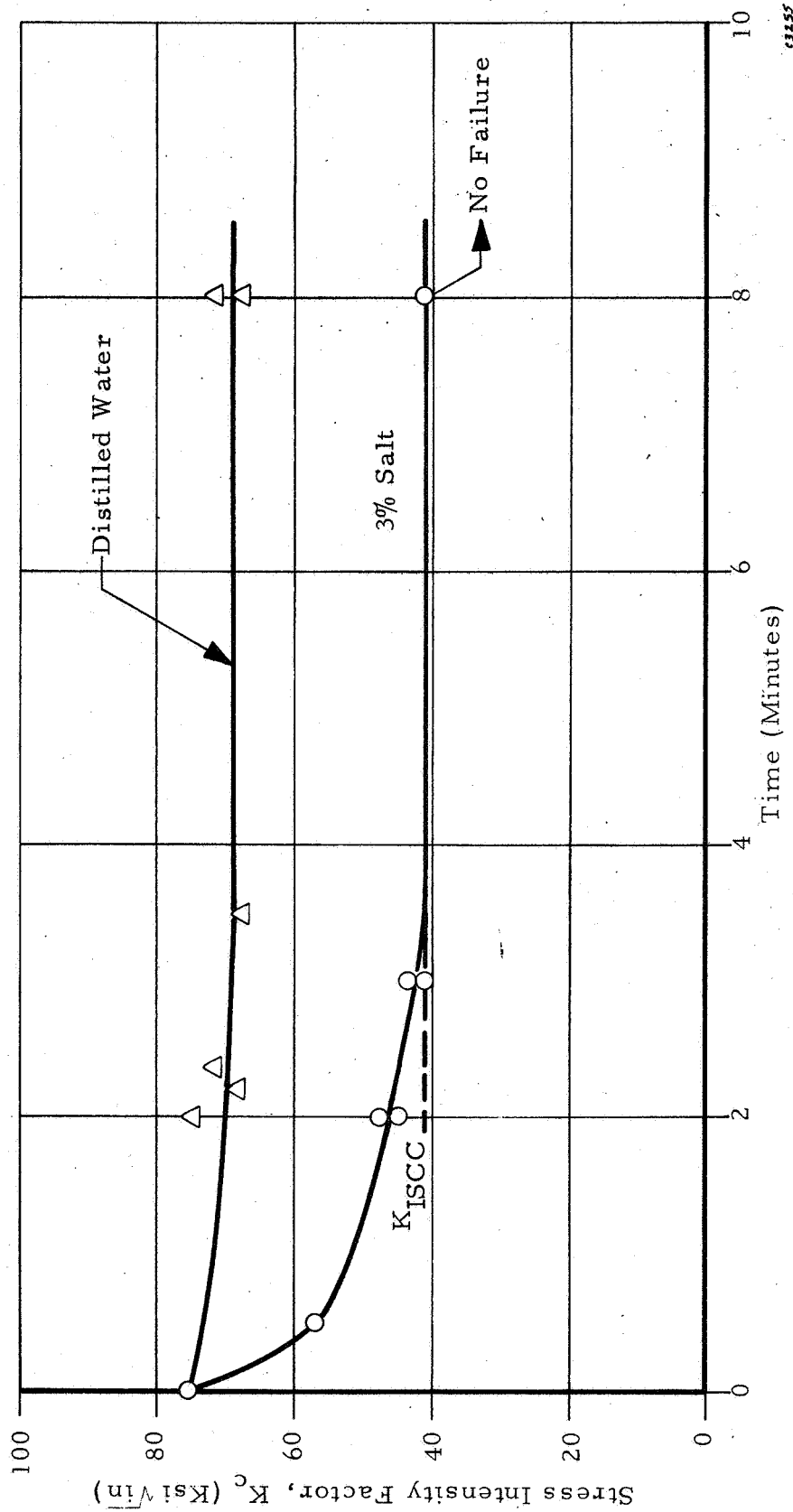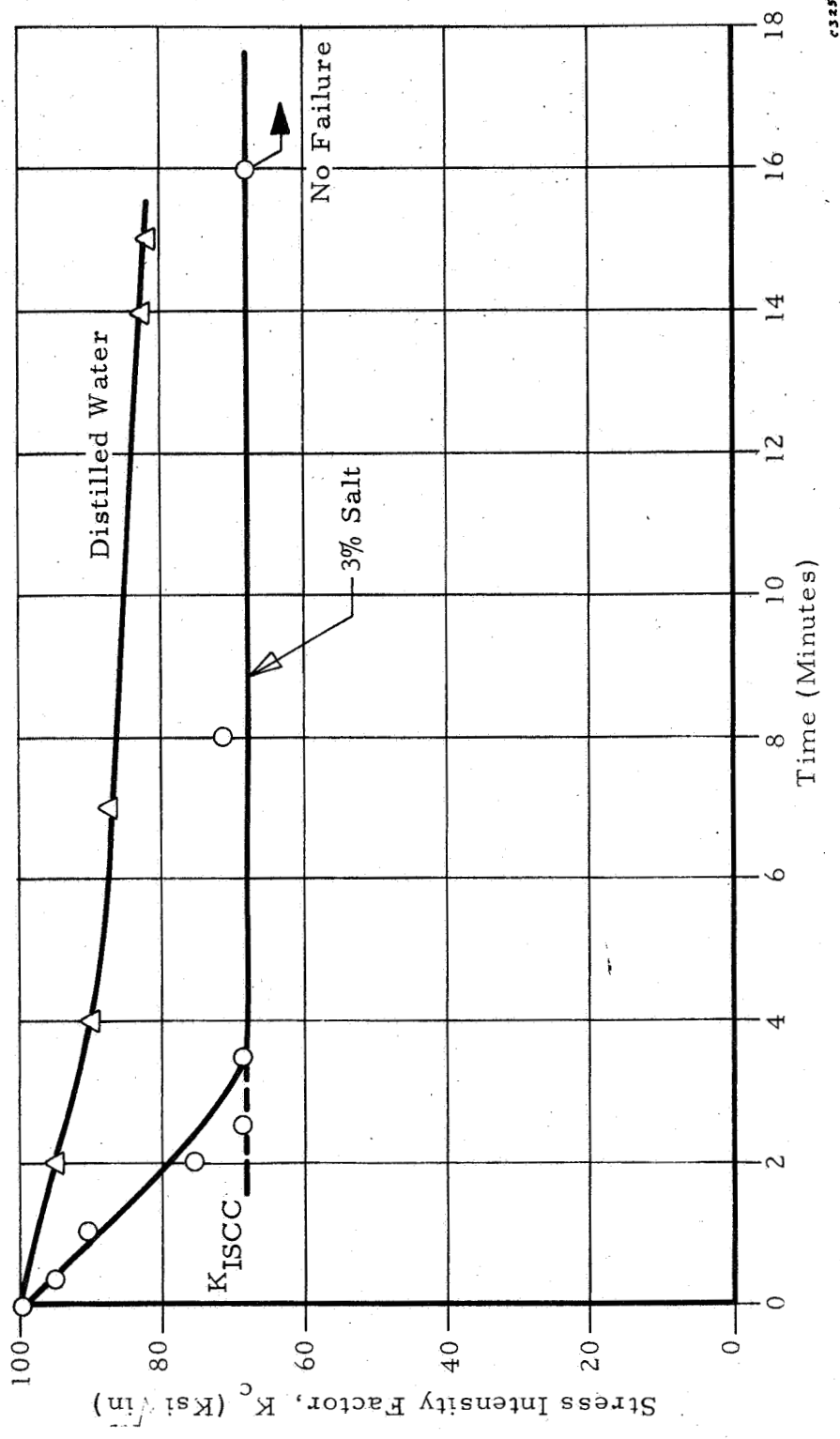Figure 8. Effect of Initial Stress Intensity on Time-To-Fracture For Ti-6Al-4V at Ambient Temperature

Figure 9. Effect of Initial Stress Intensity on Time-To-Fracture For Ti-13V-11Cr-3Al

showed that alpha alloy Ti-5Al-2.5Sn, alpha-beta alloys Ti-8Al-1Mo-1V and Ti-6Al-4V, and beta alloy Ti-13V-11Cr-3Al were susceptible to stress corrosion cracking in this environment, with the reduction of stress intensity factor for Ti-5Al-2.5Sn and Ti-8Al-1Mo-1V being much greater than for Ti-6Al-4V and Ti-13V-11Cr-3Al. Considerable reduction of stress intensity, K_c, in distilled water at ambient temperature was observed for Ti-8Al-1Mo-1V and Ti-5Al-2.5, but very little reduction was observed for Ti-6Al-4V and Ti-13V-11Cr-3Al. Two significant differences were observed between stress corrosion cracking in distilled water and 3% salt solution: (1) a higher stress intensity was required to initiate crack propagation in distilled water than in 3% NaCl solution, and (2) the crack propagation was much faster in salt solution than in distilled water.

The results of stress corrosion tests in air and 3% NaCl for the alloy Ti-8Al-1Mo-1V having Titanium Metals Heat Treat 2B2 were included in Table IV; however, examination of fracture surfaces showed that specimens failed by shear failure. The thickness of this material did not meet plain strain requirements, and the results are therefore inconclusive for this alloy.

2.4 Microfractography of Cracked Surfaces

In order to define the mode of stress-corrosion crack propagation, the fracture faces and profiles of titanium alloy samples were examined by electron microscopy replica techniques. The method of replication consisted of the two-stage carbon-plastic method. A 5% parlodion in amyl acetate was applied on the fracture face directly, or after etching. The parlodion was allowed to harden in place, stripped from the surface, deposited with carbon at a 90 degree angle, and shadowed with chrome at a 45 degree angle. The parlodion was then dissolved in acetone leaving the final Cr-C replica, which was carefully placed on electron microscope grids.

The profile of fracture faces was prepared by cleaning the test sample in distilled water, plating the fracture surface by immersion in a nickel plating bath, microsectioning and replicating the polished and etched section. The electroless nickel bath was a commercial Enthone type 410B solution. The bath acidity was adjusted to pH 4.3 to 4.5, and the bath temperature was 190 to 195°F. The plate thickness produced was 0.0025 inch. The replication

of the polished and etched surface was the two-stage carbon-plastic method similar to direct replica. The 5% parlodion in amyl acetate was applied to 200 mesh copper grids placed at the desired crack zone. After drying, the grid and plastic were stripped from the mount with scotch tape, the grids were removed, the negative replica deposited with carbon, shadowed with chromium, and the parlodion dissolved in acetone leaving the final Cr-C replica.

Figure 10 shows a two-stage Cr-C replica of an all-beta type alloy (Ti-13V-11Cr-3Al) notched specimen failed under static stress in air. Similar microstructure was noted in samples fractured in distilled water and salt solution. The fracture face is virtually all dimpled structure, indicative of ductile failure.

Figure 11 shows the fracture face of an alpha-beta alloy, Ti-6Al-4V, fractured in stress cracking in air. The fracture face exhibits ductile dimpled structure virtually throughout the surface, with some intergranular fracture facets. Figure 12 is the fractured face in stress corrosion in salt solution. The surface exhibits mixtures of cleavage and ductile regions. The cleavage areas (arrow A) are identified by river markings. The ductile areas (arrow B) are characterized by large dimples with deformation markings or serpentine glide and ripples on the surface. [6]

Attempts have been made to relate the cleavage areas to microstructure by etching the fracture surface before making the fractograph. This method has been successful in studying the hot salt stress corrosion of titanium alloys. [7] During etching many of the fracture features are removed. Figure 13 shows that with sufficient etching beta is revealed (compare Figure 13 with an unetched fracture such as Figure 12). In these experiments we have not yet taken fractographs from the same area before and after etching. However, Figure 13 does suggest one significant result. Arrow A points to a beta phase which exhibits cleavage markings.

Profile cross sections of the fracture edge were made of the Ti-6Al-4V alloy failed in air and in salt solution. The fracture in air (Figure 14) indicated transgranular ductile rupture and distortion of alpha. The fracture in salt solution (Figure 15) indicated that the crack path appears to follow alpha-beta phase boundary by cleavage, and rupture is possibly not taking

62926

Figure 10.   Electron Fractograph of Beta Alloy Ti-13V-11Cr-3Al
Fractured in Air.   Note dimple rupture.
Magnification 7,500X

c2927

Figure 11. Electron Fractograph of an Alpha-Beta Alloy
Ti-6Al-4V Fractured in Air. Note dimple
rupture. Magnification 7,500X

Figure 12.   Electron Fractograph of Stress Corrosion Region of
Ti-6Al-4V Fractured in 3% Salt Solution.   Fractograph
shows a mixture of cleavage (Arrow A) and ductile
failure (Arrow B).   Magnification 7,500X
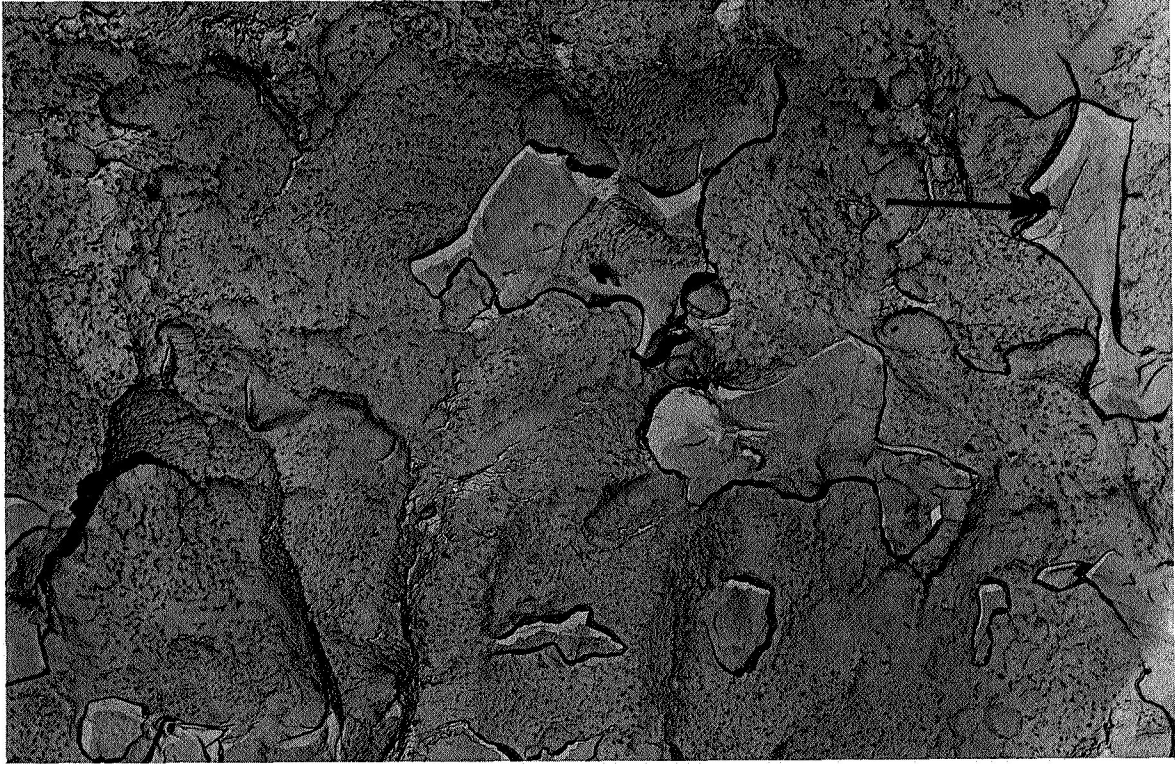
c2929

Figure 13. Electron Fractograph of Stress Corrosion Region of Ti-6Al-4V Fractured in 3% Salt Solution. Fracture has been etched for 15 seconds in HF-HNO$_3$-H$_2$O solution. Arrow points to beta phase exhibiting cleavage markings. Magnification 7,500X.
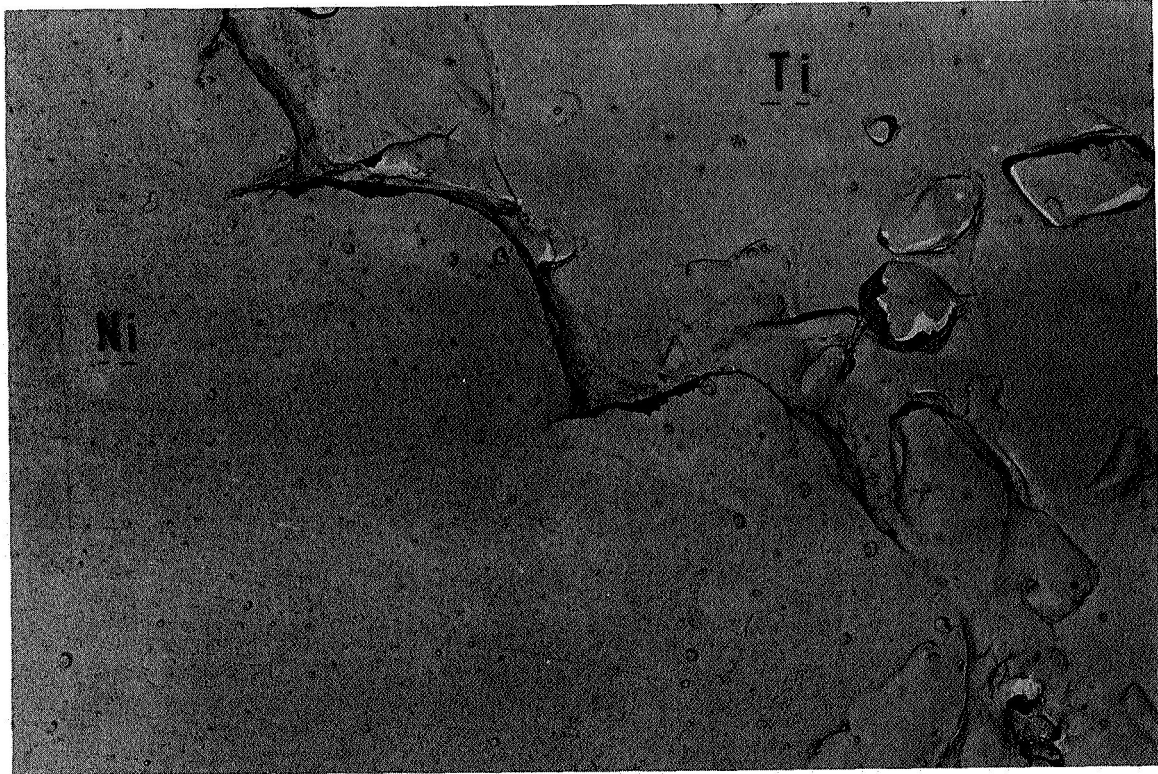
Figure 14. Profile of Fracture Edge of Ti-6Al-4V Fractured
in Air. Micrograph shows transgranular ductile
rupture. Magnification 7,500X.
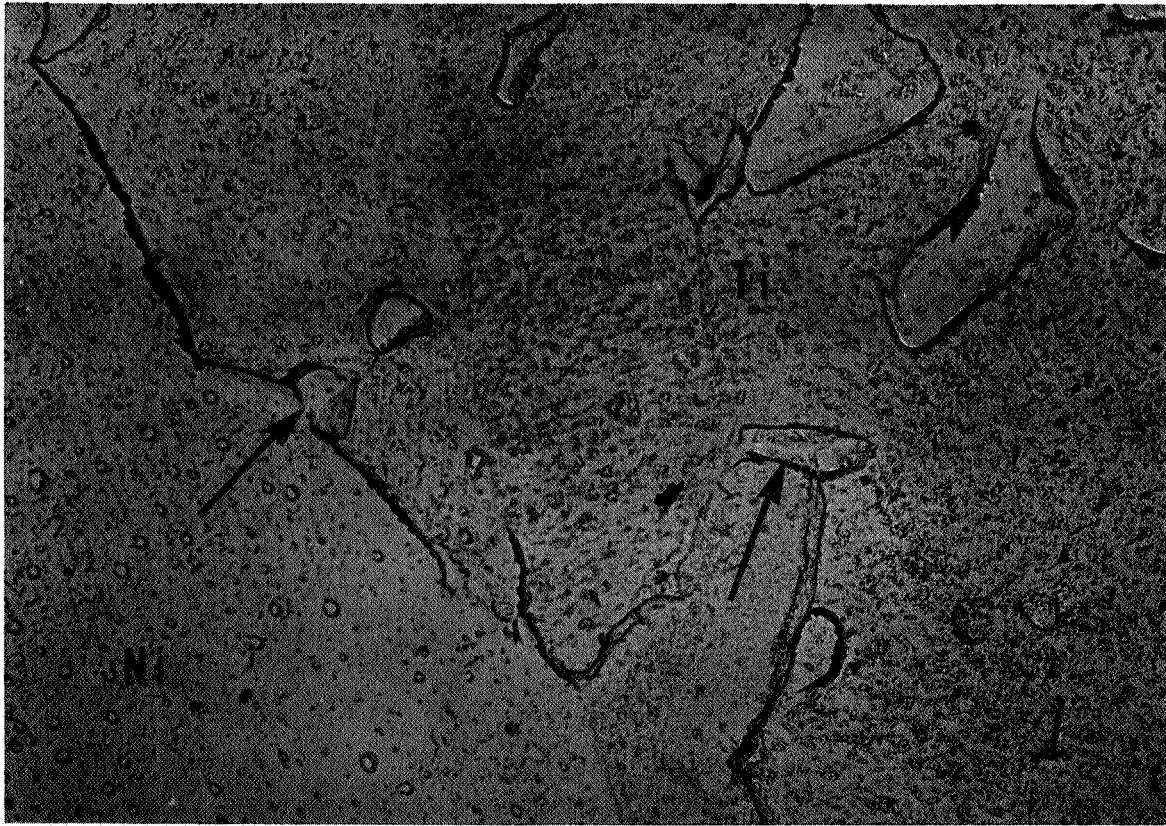
Figure 15.   Profile of Fracture Edge from Stress Corrosion
Region of Ti-6Al-4V Fractured in 3% NaCl Solu-
tion.   Fracture propagated along an alpha-beta
boundary by cleavage (Arrows).   Magnification
7,500X.

place through the beta phase. This observation is contrary to the results reported by Beck[10] that failure in Ti-8Al-1Mo-1V alloy under SCC condition occurs by apparent cleavage in the alpha phase and ductile failure of the beta phase. It is apparent that hydrogen segregation in the beta phase as demonstrated in Section 2.3, might be associated with the type of cleavage failure of the alpha-beta phase boundary described here. Further work along these lines will be of great benefit in clarifying the nature of cleavage.

The fracture faces of the Ti-8Al-1Mo-1V alloy failed in distilled water and salt solution exhibited similar morphology to the Ti-6Al-4V alloy. Figures 16 and 17 show mixtures of local cleavage and ductile rupture areas. There was also some evidence of intergranular fracture regions for this alloy.

The fracture surface of the alpha type alloy, Ti-5Al-2.5Sn, failed in air, is shown in Figure 18. The fracture face predominantly shows dimple rupture (arrow A), and some evidence of (serpentine) glide and deformation markings (arrow B), characteristic of ductile fracture.[21] The microfractograph of specimens failed in distilled water showed predominantly ductile rupture with some local cleavage areas (Figure 19). The salt water stress corrosion fracture face exhibited much larger areas of cleavage distributed throughout the surface, as illustrated in Figure 20.

Also examined were profile cross sections of the alpha alloy, Ti-5Al-2.5Sn, failed in air and salt solution. Figure 21 shows ductile transgranular fracture in air with distorted alpha grains. There was some indication that the fracture path followed along alpha grain boundaries where retained beta was formed. Specimens fractured in the salt solution exhibited less distortion of the alpha phase, and cleavage along the alpha-beta boundaries (Figure 22). The cleavage areas from salt solution fracture are considerably larger in size than the retained beta phase observed in the profiles; however, in distilled water the cleavage areas are comparable in size with the retained beta.

2.5 Microautoradiography Studies

2.5.1 Preferred Hydrogen Distribution in Titanium Alloys

Hydrogen is the most likely embrittling species to be absorbed from an aqueous environment, since H_2 gas is produced at cathodic

SM-49105-F1

c-2932

Figure 16. Electron Fractograph from Stress Corrosion Region
of Ti-8Al-1Mo-1V Fractured in 3% Salt Solution.
Fractograph shows ductile rupture (Arrow A),
cleavage (Arrow B) and evidence of intergranular
fracture (Arrow C).   Magnification 7,500X.
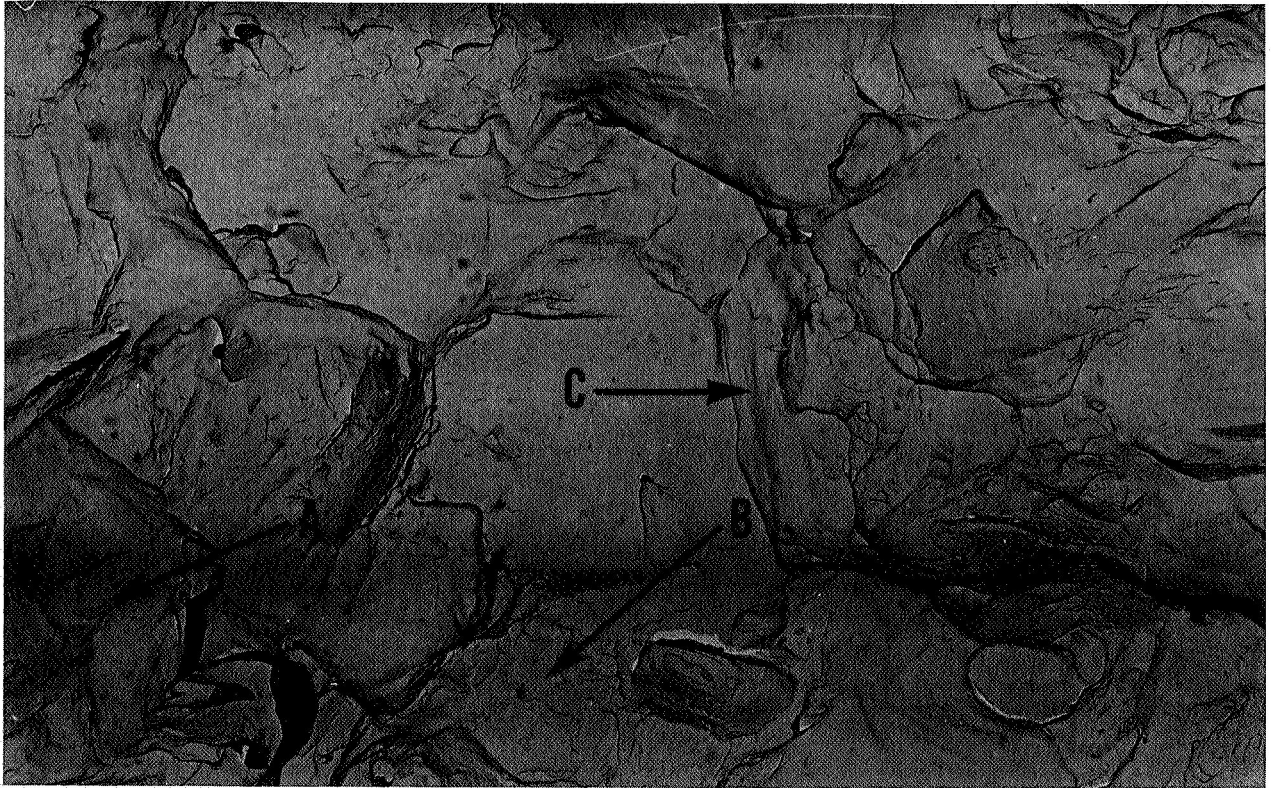
C2933

Figure 17. Electron Fractograph from Stress Corrosion Region
of Ti-8Al-1Mo-1V Fractured in Distilled Water.
Fractograph shows ductile rupture (Arrow A),
cleavage (Arrow B), and evidence of intergranular
fracture (Arrow C).   Magnification 7,500X.

02934

Figure 18. Electron Fractograph of Air Fractured Surface of
Ti-5Al-2.5Sn. Fractograph shows dimple rupture
(Arrow A), and glide characteristic of ductile
fracture (Arrow B). Magnification 7,500X.

Figure 19.   Electron Fractograph from Stress Corrosion Region
of Ti-5Al-2.5Sn Fractured in 3% NaCl.   Fractograph
shows cleavage area (Arrow A).   Most of the fracture
exhibits ductile failure with these local cleavage areas
distributed throughout.   Magnification 7,500X.
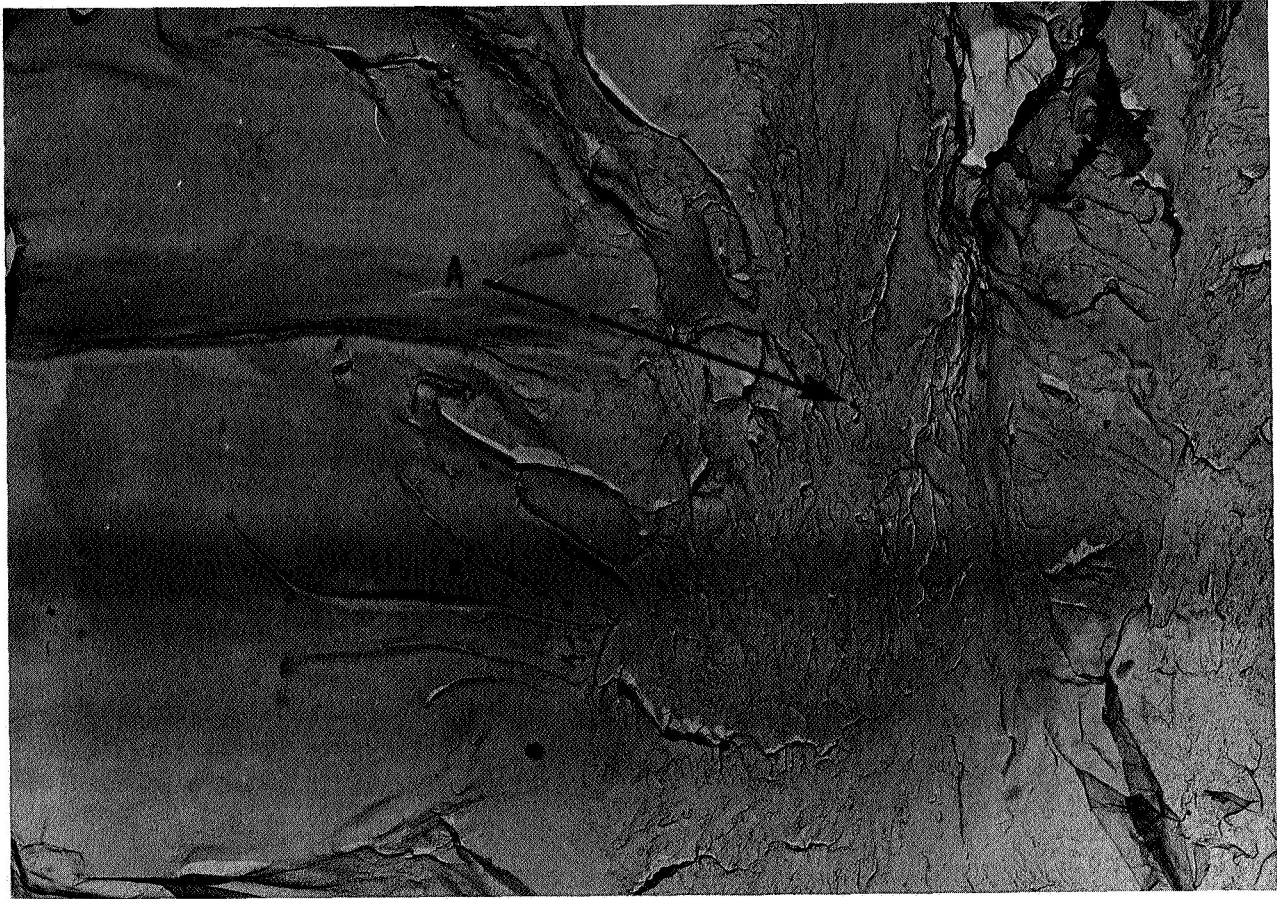
C2936

Figure 20. Electron Fractograph from Stress Corrosion Region
of Ti-5Al-2.5Sn Fractured in Distilled Water. Most
of the fracture exhibits ductile failure (Arrow A) in
its local cleavage areas distributed throughout
(Arrows B). Magnification 7,500X.
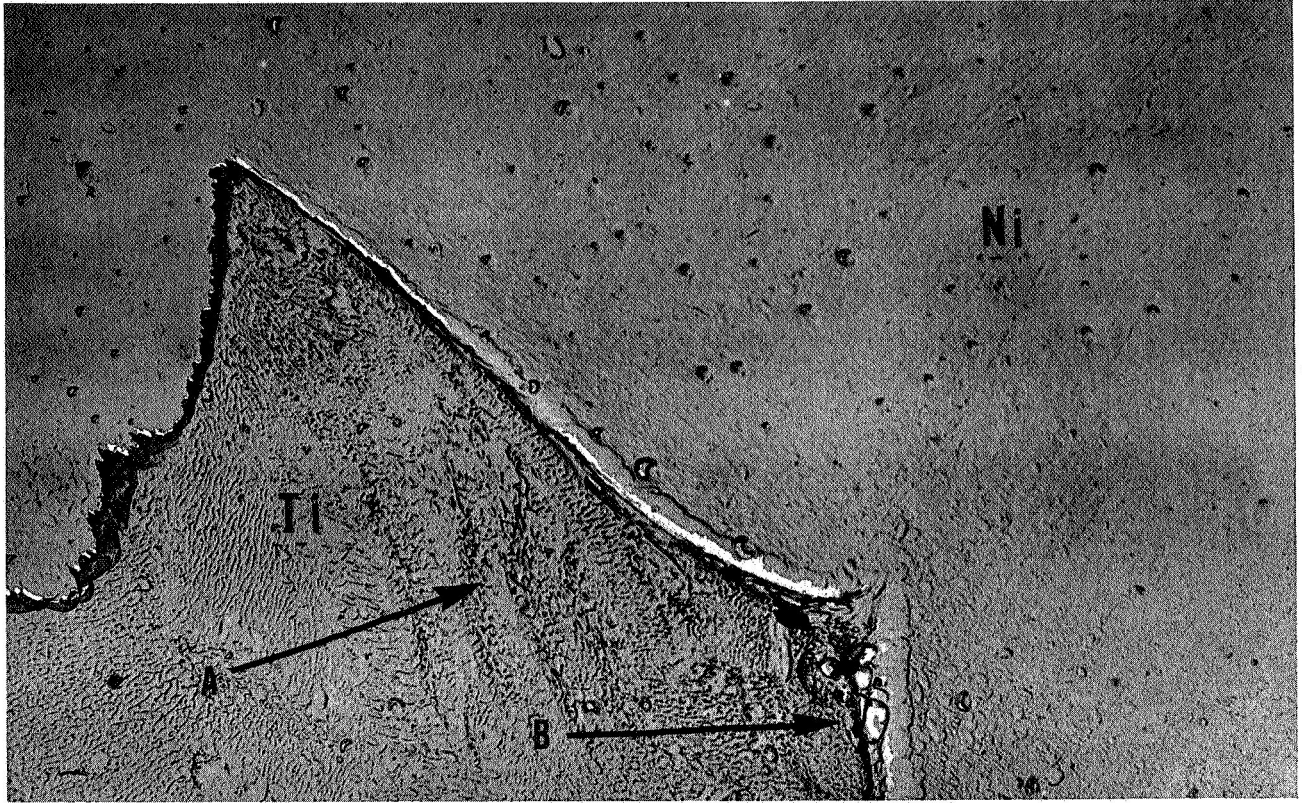
Figure 21. Profile of Fracture Edge of Ti-5Al-2.5Sn Fractured
in Air. Arrow A shows deformed region of alpha,
and Arrow B shows failure along an alpha-beta
interface. Magnification 7,500X.

Figure 22. Profile of Fracture Edge in Stress Corrosion Region
of Ti-5Al-2.5Sn Fractured in 3% NaCl Solution. In
this region (Arrows A), fracture propagated along an
alpha-beta interface. Beta particles were precipitated
in alpha grain boundaries. Magnification 7,500X.

sites. The solubility of H_2 at room temperature is much lower in the alpha phase than in the beta-phase, but it is strongly dependent on alloy content. For instance, in titanium-aluminum (α), the H_2 solubility increases from 1 to 2 ppm for pure titanium to 400 ppm for Ti-7Al.[22]

There have been few attempts to determine the preferential distribution of hydrogen in titanium alloys. Huber et al[23] introduced tritium into a Ti-3Mn-1Fe-1Cr-1Mo-1Fe alloy and observed the tritium distribution after heat treatment using autoradiography. They found that hydrogen concentrates in alpha-beta boundaries in the form of hydrides after duplex heat treatments involving aging in the 800 to 1200°F range. There also was some evidence that hydrogen partitioned to the beta-phase in preference to the alpha phase.

To study the preferential distribution of hydrogen in the various titanium alloys selected and its role in stress corrosion cracking by electron microautoradiography technique, the radioactive hydrogen (tritium) was introduced into the alloy samples by two methods: (1) gas adsorption at elevated temperature, and (2) cathodic charging. The studies on cathodic charging were not conclusive, and the results on gas adsorption of tritium at elevated temperatures were examined in detail and are described here.

Tritium gas was introduced into each of the four titanium alloys employing a modified Sieverts apparatus designed and fabricated by Astropower Laboratory as shown in Figure 23. The apparatus is comprised of a forepump, two-stage mercury diffusion pump, ion gage, McLeod gage, tritium inlet system, and sample tubes. A mercury cut-off is used to isolate the vacuum manifold from the diffusion pump. The McLeod gage is accurately calibrated and covers the pressure range from 10^{-3} to 1 torr. The ion gage was used only to determine the ultimate vacuum obtainable in the system during initial outgassing and pump down. The tritium inlet system employs a mercury-sealed fritted glass disc valve to admit the tritium to the vacuum manifold. Individual samples 1/4 inch by 1 inch were pickled in an aqueous solution of HNO_3-HF and placed in vertical Vycor tubes which were attached to the Pyrex manifold using graded seals. With the manifold isolated from the vacuum pumps by the mercury cut-off, the total volume of the manifold was determined by expanding a known pressure of air (approximately 1 torr)
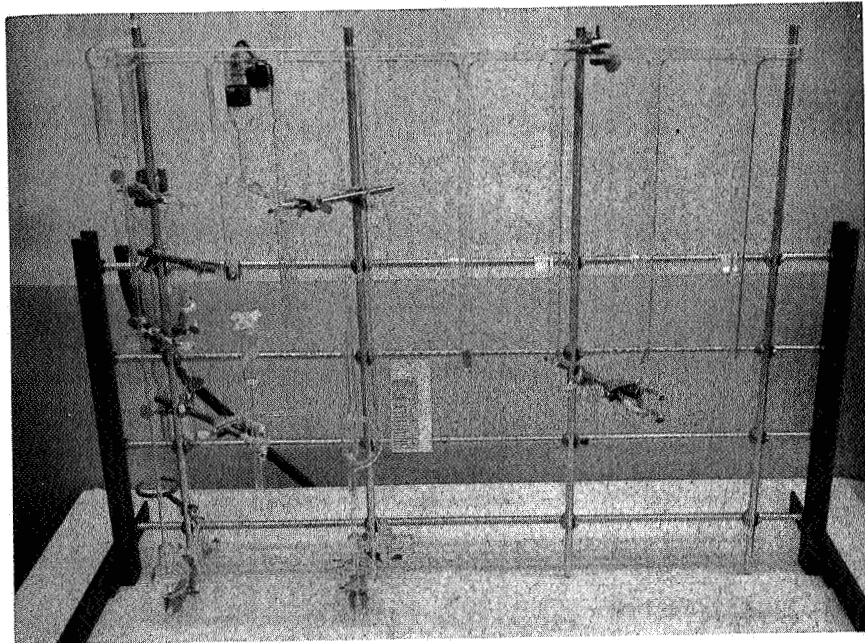
c2595

Figure 23. Modified Sieverts Apparatus for Charging
Tritium in Titanium Alloys

from the known volume of the McLeod gage tube to the manifold. The pressure was remeasured — with the McLeod gage — and the system volume calculated from gas law.

In order to charge titanium alloys, the Vycor tubes containing an alloy sample were evacuated to 10^{-7} and heated to $725^{\circ}C \pm 10^{\circ}C$, and held at this temperature until degassing was completed in about 1/2 hour. The specimen tube was cooled to ambient temperature, carrier-free tritium gas was added and the tube was reheated to $725^{\circ}C$ until a final steady static pressure was attained in the system. The specimen tube was then cooled to ambient temperature and the final pressure was measured. The operation was repeated for each alloy until all the samples were charged. The amount of carrier free tritium introduced into each alloy as estimated from the pressure drop is shown in Table V. The accuracy of the measurements by this technique is within 5%.

Before describing results, a brief description of the characteristics of tritium in titanium should be discussed. Tritium is a beta emitter with a half life of 12.26 years. The beta particle has a maximum energy of 0.018 MeV and has a certain significant depth of penetration in titanium of about .18 micron (see Appendix A). Thus all tritium in the metal deeper than .18 micron will not be recorded on the emulsion. Furthermore, since a beta particle may emit in any direction, this means that the maximum resolution is about .06 micron, i.e., any silver filament observed on the radiograph must be within .06 micron of the actual location of the tritium nuclei that emit the beta particle which caused that particular silver filament.

The electron microautoradiographs of titanium alloys charged with tritium at $725^{\circ}C$ were prepared as follows:

1. Ten angstroms of chromium were shadowed at 20 degrees. The chromium was placed on the specimen to act as a shadow for the direct carbon replica.

2. 150 angstroms of carbon were deposited onto the titanium for a direct replica of the metal surface.

3. A monolayer of Kodak NTE nuclear track emulsion was then placed on the surface.

4. The specimens were exposed for 16 hours.

5. The emulsion was developed while on the specimen and fixed.

TABLE V

CONCENTRATION OF TRITIUM ADDED TO TITANIUM ALLOYS

Alloy	Concentration (ppm)
Ti-5Al-2.5Sn	48
Ti-6Al-4V	41
Ti-8Al-1Mo-1V	43
Ti-13V-11Cr-3Al	43

6. The carbon replica and emulsion were removed with nitric acid and hydrofluoric acid.

7. The autoradiograph was rinsed, dried, and examined in the electron microscope.

2.5.1.1 Observations on Ti-13V-11Cr-3Al Alloy

Tritium was evenly distributed throughout the lattice of this all-beta alloy. There was no apparent concentration at boundaries. Figure 24 is a microautoradiograph showing distribution of tritium in two different beta grains of Ti-13V-11Cr-3Al alloy.

2.5.1.2 Observations on Ti-8Al-1Mo-1V and Ti-6Al-4V Alloys

The tritium distribution in Ti-8Al-1Mo-1V and Ti-6Al-4V alpha-beta alloys was very similar. Most of the tritium was concentrated in the beta phase of these two alloys. Figures 25 and 26 show the results of this experiment.

2.5.1.3 Observations on Ti-5Al-2.5Sn Alloy

Charging of 48 ppm of tritium gas at 725°C and subsequent air quenching produced extensive cracking in this alpha alloy as shown in Figure 27. Examination of the microstructure of metal in the region of the crack showed that the fracture was intergranular. A microautoradiograph of this alloy showed a uniform distribution of tritium in the alpha grains, but a high concentration of tritium in a second phase at grain boundaries. Figure 28 shows the results of this experiment. The second phase is retained beta phase in alpha grain boundaries.

Attempts were made to determine the concentration of tritium in beta phase of alpha-beta alloys shown in Figures 26, 27 and 28 by counting the filaments on the electron microautoradiographs, and by calculating the efficiency of the nuclear track emulsion to the beta particles of radioactive tritium. The efficiency of the nuclear track emulsion was estimated using the specimen of Ti-5Al-2.5Sn with 48 ppm tritium as the reference material (see Appendix A). The concentration of atoms causing these filaments is calculated by the expression
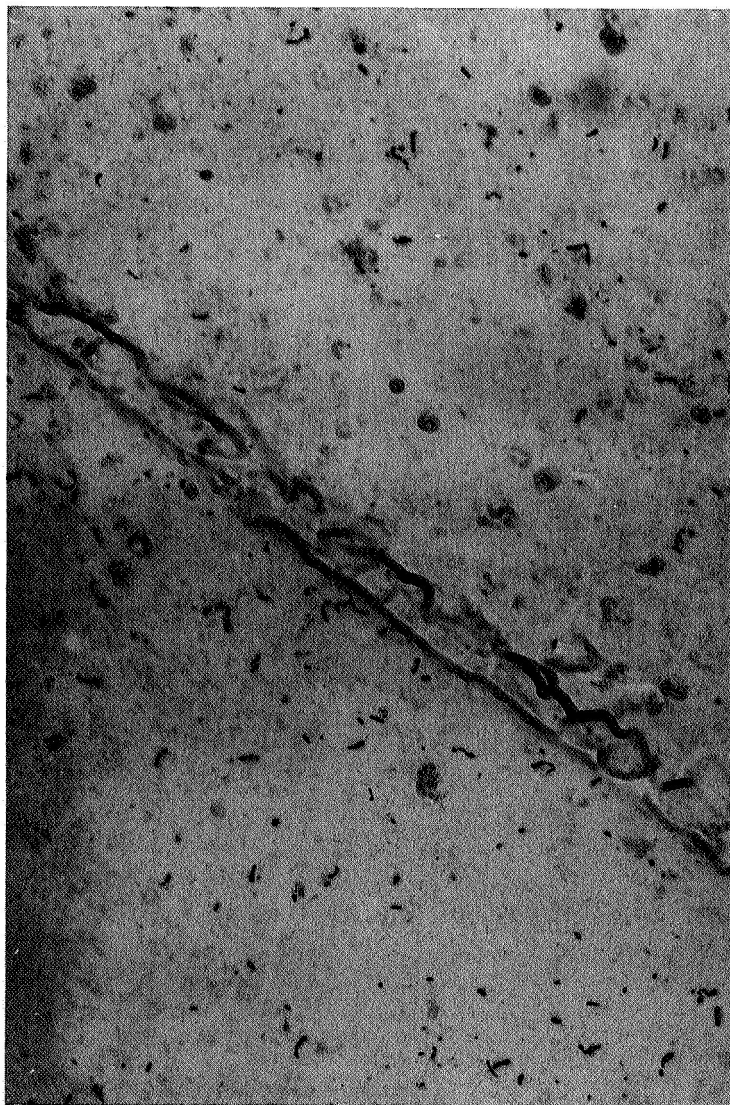
c.2921

Figure 24. Microautoradiograph of Tritium in
Ti-3Al-13V-11Cr. Magnification
20,000X.
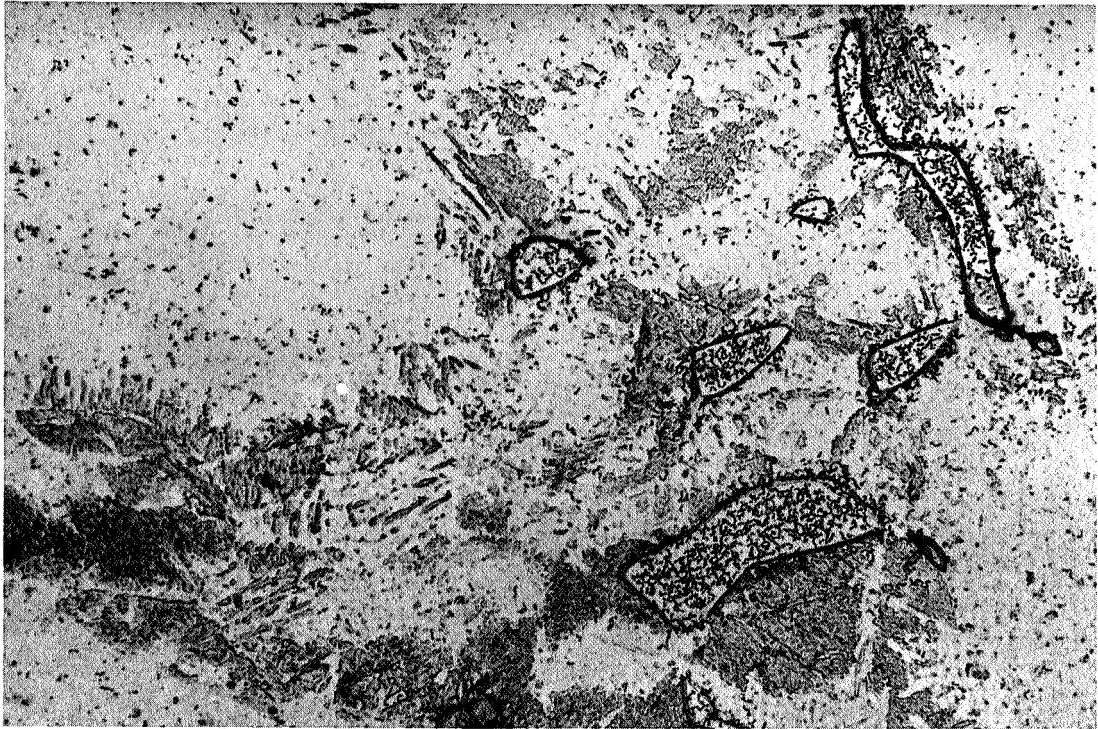
(a)
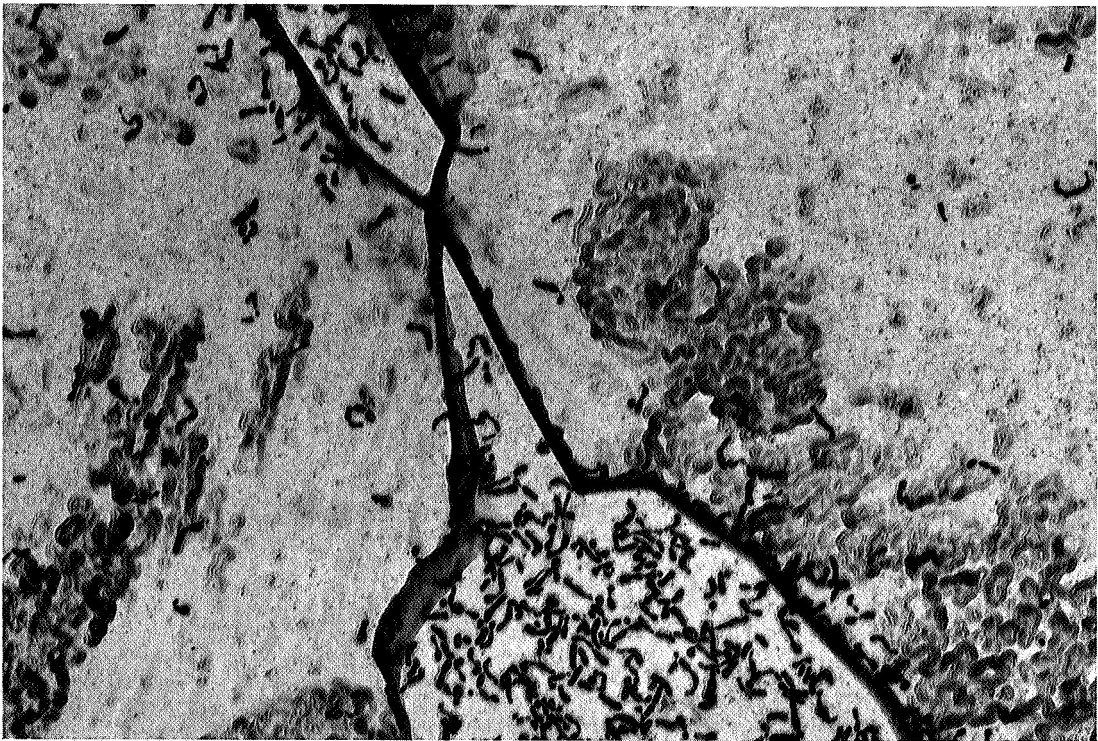
(b)

(a)   8,000X
(b) 30,000X

Figure 25. Microautoradiographs of Tritium in Ti-8Al-1Mo-1V.
Tritium is concentrated in beta phase.
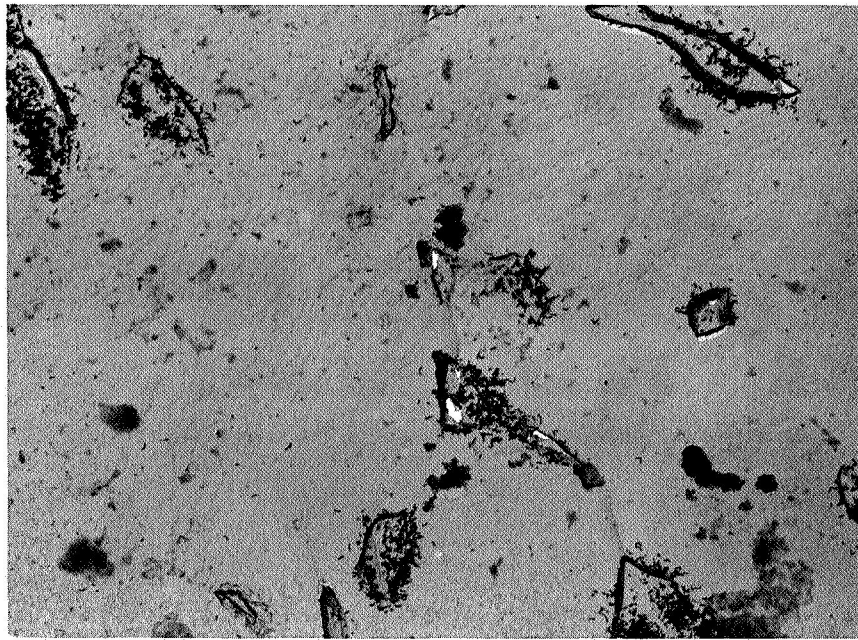
(a)
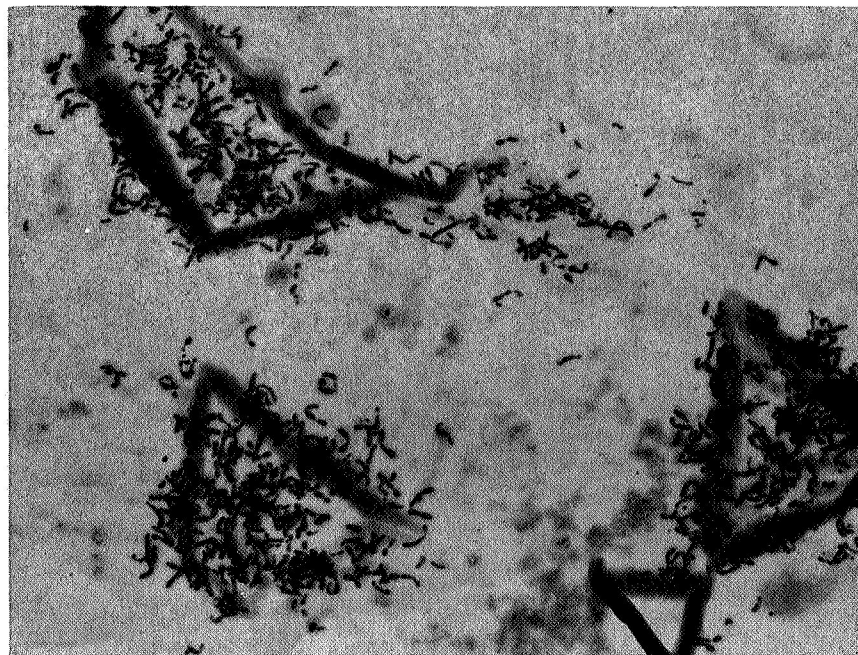
(b)

C2923

(a) 4,500X
(b) 15,500X

Figure 26. Microautoradiograph of Tritium in Ti-6Al-4V.
Tritium is concentrated in the beta phase.

C2924

Figure 27. Development of Cracks in Ti-5Al-2.5Sn Due
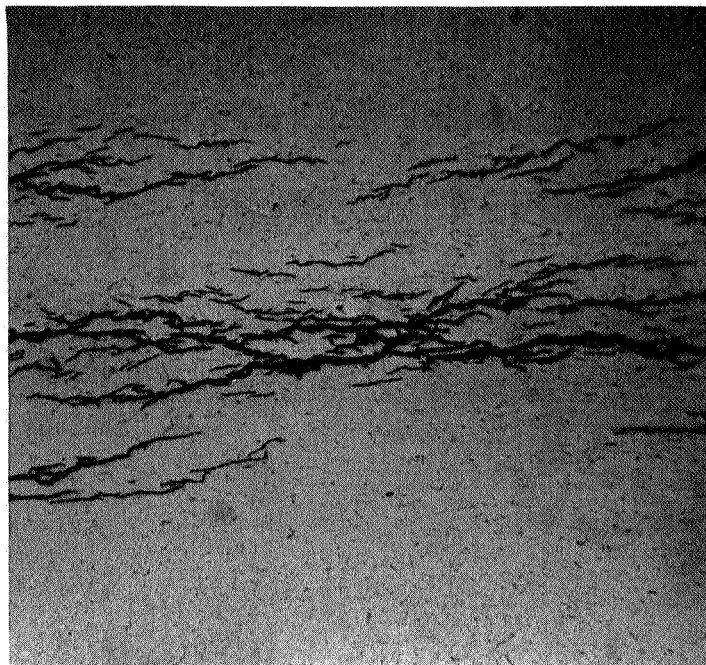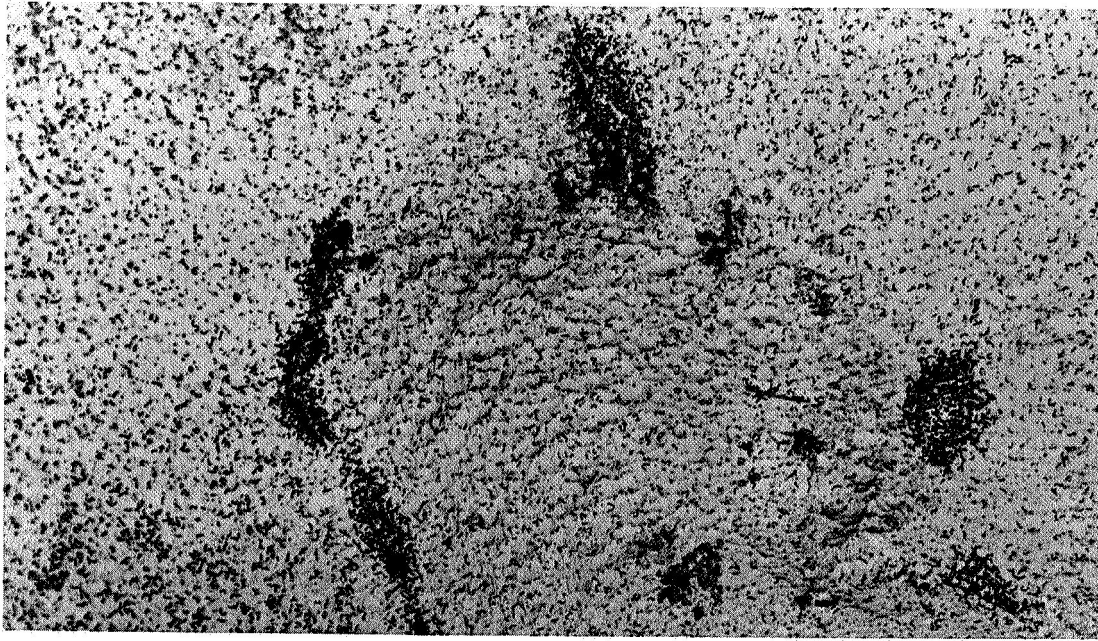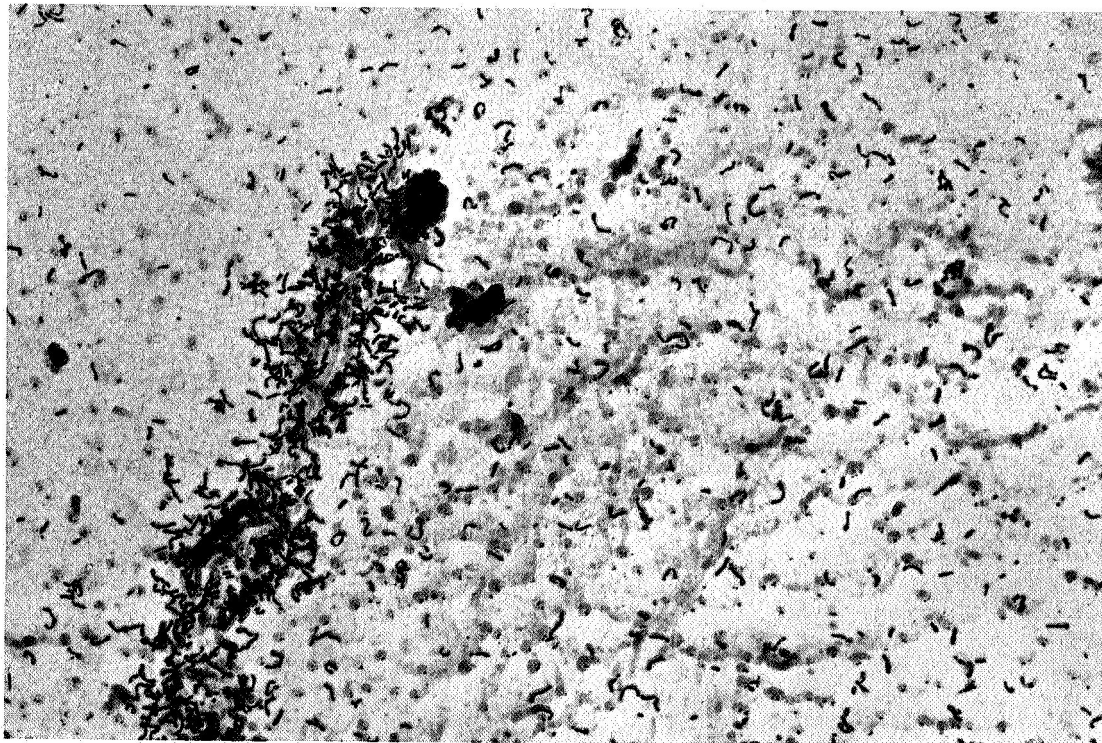to Charging of 48 ppm Tritium at 725°C.
Magnification 175X

(a)

(b)

c2925

(a)   6,000X
(b) 30,000X

Figure 28.   Microautoradiograph of Tritium in Ti-5Al-2.5Sn.
Tritium is concentrated at beta precipitated in
alpha grain boundaries.

$$\text{fraction of } H^3 \text{ to total weight} = \frac{\text{no. of filaments/cm}^2}{\text{emulsion efficiency}} \times \text{disintegration/fil}$$

$$\times \frac{1}{\lambda t} \times \frac{\text{atomic weight}}{6.02 \times 10^{23}} \times \frac{1}{\text{effective range of } \beta \text{ in metal}}$$

where λ is the disintegration constant for tritium and t is the exposure time (16 hours).

For H^3 in titanium alloys, this expression becomes

$$\text{ppm of } H^3 = \frac{\text{no. of filaments/cm}^2}{\text{emulsion efficiency}}$$

$$\times \left[\frac{3 \times 10^6}{(.131)(1.82 \times 10^{-9})(5.76 \times 10^4)(6.02 \times 10^{23})(.08 \times 10^{-3})} \right]$$

$$\text{ppm of } H^3 = 4.55 \times 10^{-9} \left[\frac{\text{number of filaments/cm}^2}{\text{emulsion efficiency}} \right]$$

The concentration of tritium in the beta phase was calculated using an emulsion efficiency of 18%.

The results are shown in Table VI. It will be noted that if a titanium alloy contains approximately 40 ppm of hydrogen, the beta phase may contain several hundred ppm. This may be quite significant. Quigg and Troiana[24] have shown that the beta phase of composition, Ti-13V-11Cr-3Al becomes embrittled if the hydrogen content is greater than 420 ppm. The beta phase in other alloys is not of this composition, so the exact level of hydrogen needed for embrittlement would be somewhat altered. The results of microautoradiography analysis, however, suggest that the beta phase in Ti-5Al-2.5Sn and in Ti-8Al-1Mo-1V is close to the hydrogen content necessary for embrittlement.

2.5.2   Effect of Stress to Hydrogen Distribution

Titanium alloys of $\alpha + \beta$ type are known to be susceptible to slow-strain-rate H_2 embrittlement. Failure has been postulated to be caused by a strain-induced precipitation of hydride.[25] Crack growth

TABLE VI

CONCENTRATION OF TRITIUM IN BETA PHASE OF
Ti-5Al-2.5Sn, Ti-6Al-4V AND Ti-8Al-1Mo-1V

Alloy	Filaments/cm^2	ppm H^3	Average ppm
Ti-5Al-2.5Sn	184×10^8	460	428
	164×10^8	410	
	160×10^8	400	
	176×10^8	440	
Ti-6Al-4V	109×10^8	272	285
	118×10^8	295	
	101×10^8	252	
	122×10^8	305	
	121×10^8	302	
Ti-8Al-1Mo-1V	196×10^8	490	455
	170×10^8	425	
	210×10^8	525	
	164×10^8	410	
	170×10^8	425	

could result from fracture of brittle hydride in the α phase or selective dissolution along slip planes due to hydride precipitation in alpha-beta alloys.

An experiment was made to study the distribution of hydrogen in alpha-beta and beta alloys at the crack tip of stressed single-edge notch specimens with fatigue cracks. Specimens described in Section 2.2 were used for this experiment. Thirty ppm of tritium was added by gas absorption to specimens of Ti-5Al-2.5Sn and Ti-6Al-4V. Seventy-two ppm of tritium was added to a specimen of Ti-13V-11Cr-3Al. The specimens were placed in loading jigs and stressed in air and held for a period of twenty-four hours before applying the nuclear track emulsion.

Since it was desirable to observe the hydrogen distribution at the crack tip, a better method of stripping the emulsion from the surface was required.

The electron microautoradiographs of stressed tritiated titanium alloy specimens were prepared as follows:

1. The specimens were initially stressed in a loading jig for a period of 24 hours.

2. The loading jig is placed in a vacuum chamber. Ten angstroms of 80% Pt-20% Pd alloy were deposited to act as a shadow and 150 angstroms of carbon were deposited for direct replica onto the specimen surface.

3. The specimen is transferred to the dark room and a monolayer of Kodak NTE nuclear track emulsion was then placed on the surface, and the specimen was exposed for 16 hours.

4. The specimen was removed from stress jig. The emulsion was developed while on the specimen and fixed.

5. Three layers of 5% Parlodion were placed on surface and allowed to dry, and electron microscope grids were placed in the fourth layer.

6. Parlodion plus emulsion was mechanically stripped from surface, and Parlodion substrate dissolved in amyl acetate.

Initially all of the specimens were stressed to a stress intensity level of 25 ksi $\sqrt{in}$. The beta alloy specimen unexpectedly broke while applying the load. Visual examination of the specimen indicated that fracture was of a brittle nature; however, a detailed study was not made. A microautoradiograph was

made of this specimen using procedure described above (see Figure 29). The filament density for this specimen was 19×10^8 filaments/cm^2 which compares favorably with the filament density, 9×10^8 filaments/cm^2 for specimen with 43 ppm, obtained by acid stripping technique.

The Ti-5Al-2.5Sn and Ti-6Al-4V specimens were examined at 25 ksi $\sqrt{\text{in}}$. and 50 ksi $\sqrt{\text{in}}$. stress intensity levels, which are stress intensity levels below and above value for stress corrosion in aqueous salt solutions.

The stress distribution around a crack tip is dependent on the mode of loading and the stress state. In the single edge notch specimen of this study, the surface which the radiograph is placed on, is under a plane stress condition. The load causes a predominately Mode I displacement. For these conditions the stresses around the crack tip are:

$$\sigma x = \frac{K_I}{(2 \pi r)^{1/2}} \cos \frac{\theta}{2} \left[1 - \sin \frac{\theta}{2} \sin \frac{3\theta}{2} \right]$$

$$\sigma y = \frac{K_I}{(2 \pi r)^{1/2}} \cos \frac{\theta}{2} \left[1 + \sin \frac{\theta}{2} \sin \frac{3\theta}{2} \right]$$

$$\tau xy = \frac{K_I}{(2 \pi r)^{1/2}} \sin \frac{\theta}{2} \cos \frac{\theta}{2} \cos \frac{3\theta}{2}$$

$$\sigma z = \tau xz = \tau yz = 0$$

K_I is the stress intensity factor

These equations apply only in the elastic range when r is small compared to specimen dimensions. If yielding takes place at the crack tip, the stress distribution will be modified. Figure 30 is a plot of these stresses for specimens loaded to the $K_I = 26$ ksi $\sqrt{\text{in}}$. value.

The microautoradiographs of the entire grid samples around fatigue crack tip did not show any redistribution of tritium in the alpha matrix or in the beta phase at the stress intensity levels of 25 and 50 ksi $\sqrt{\text{in}}$. of Ti-5Al-2.5Sn and Ti-6Al-4V. The typical results for Ti-5Al-2.5Sn and Ti-6Al-4V are illustrated in Figures 31 through 33.
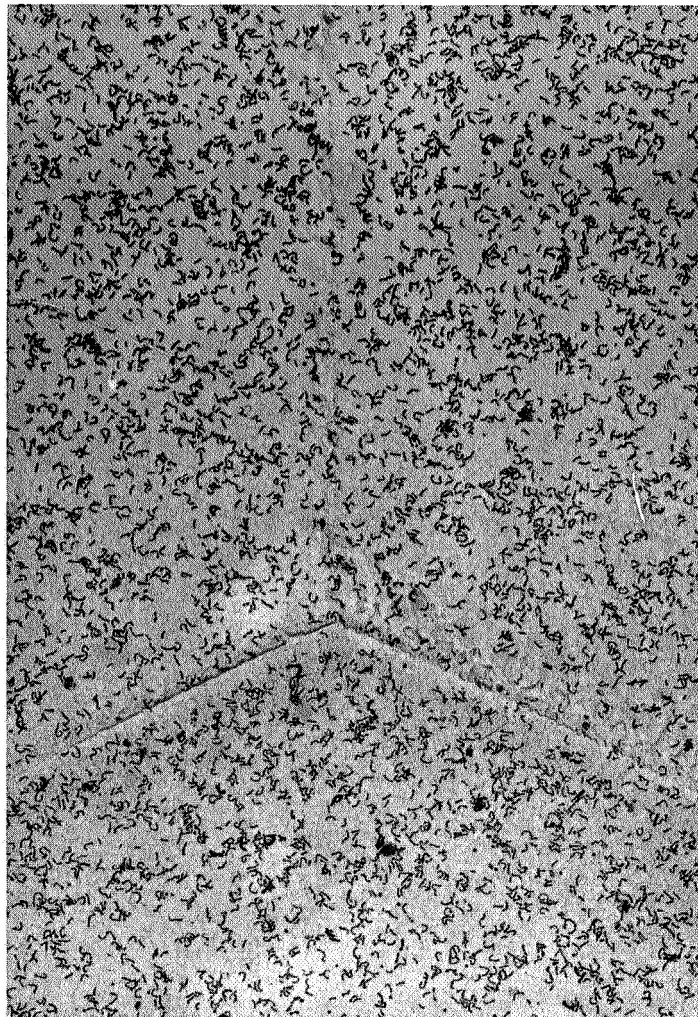
c3250

Figure 29.   Microautoradiograph of Tritium in Ti-13V-
11Cr-3Al (72 ppm).   Magnification 8,375X.
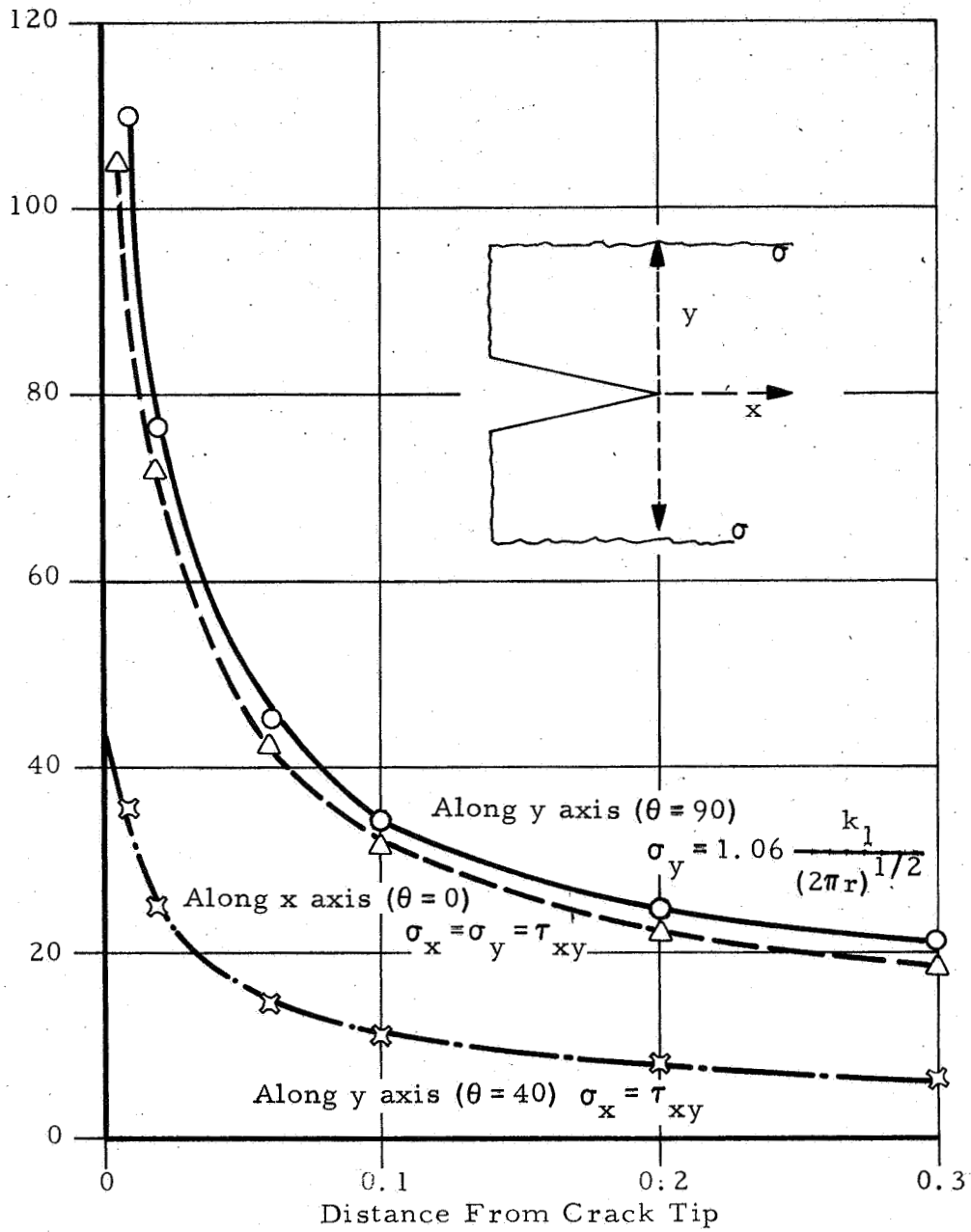
Figure 30. Stress Distribution Around a Crack Tip For $K_I = 26$ ksi $\sqrt{\text{in.}}$

Fatigue Crack
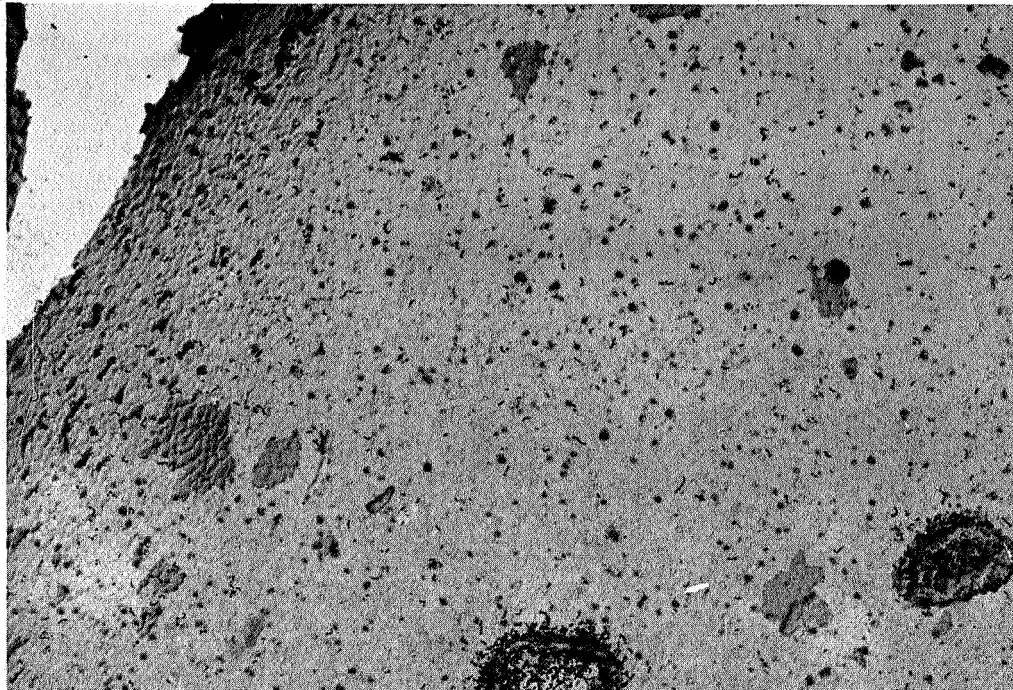
c3249

Figure 31.   Microautoradiograph of Stressed Single Edge
Notched Precracked Tritiated Ti-5Al-2.5Sn
Specimen, Stress Intensity 50 ksi $\sqrt{\text{in}}$.
Magnification 10,000X.
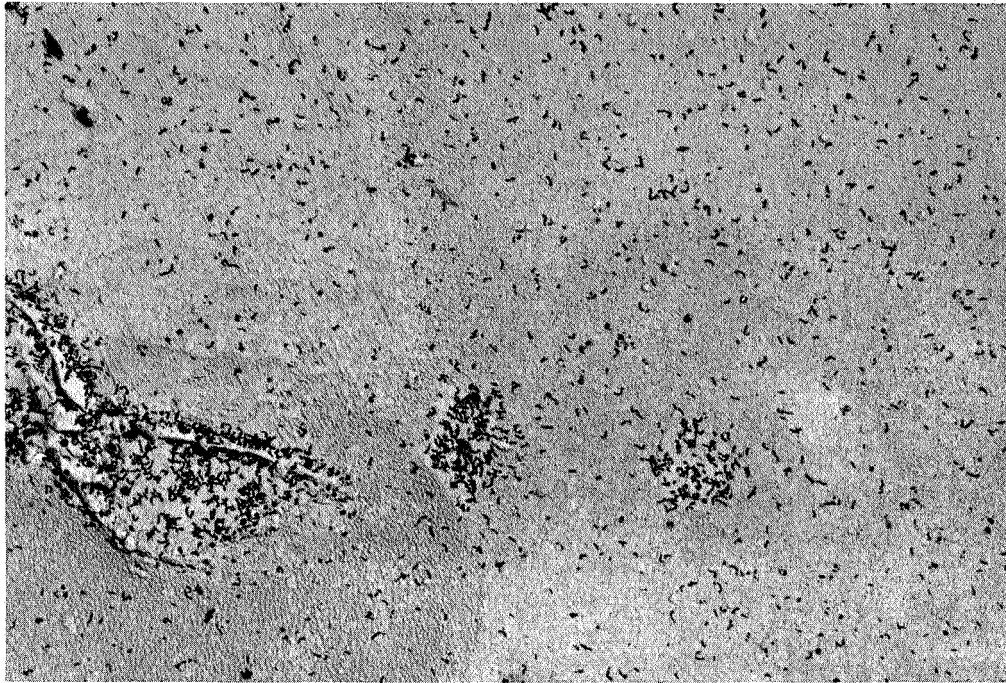
c3251

Figure 32. Microautoradiograph of Tritium in Ti-5Al-Sn Within 0.001 Inch of Fatigue Crack Single Edge Notched Specimen, Stress Intensity 25 ksi $\sqrt{\text{in}}$. Magnification 10,000X.

C3252

Figure 33. Microautoradiograph of Tritium in Ti-6Al-4V Within 0.001 Inch of Fatigue Crack Single Edge Notched Specimen, Stress Intensity 50 ksi $\sqrt{in}$. Magnification 10,000X.

c3253

Figure 34. Microautoradiograph of Tritium in Ti-6Al-4V
at Crack Tip of Fatigue Crack Single Edge
Notched Specimen, Stress Intensity 25 ksi√in.
Magnification 10,000X.

2.6   Electrochemical Evaluations

Electrochemical studies were conducted in order to evaluate the possible electrochemical reactions that should be considered during the stress corrosion of Ti alloys. The studies were limited to mill annealed Ti-6Al-4V and Ti-5Al-2.5Sn. The effect of oxygenation and stress were evaluated.

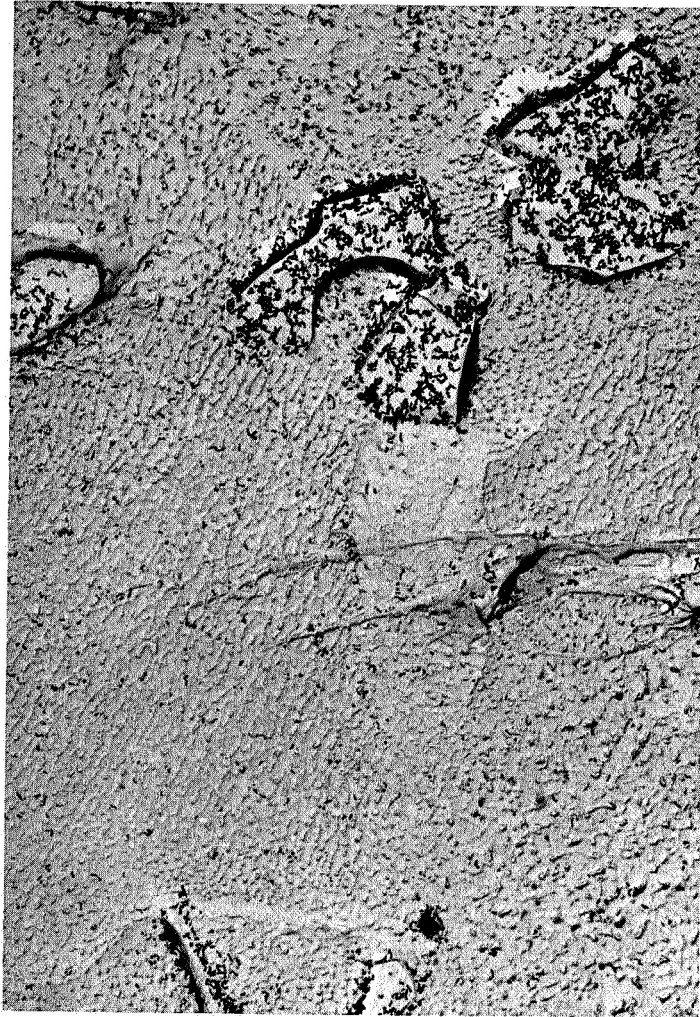Sheet tensile specimens, 0.025 inch thick, were abraded with 600 grit silicon carbide and then coated with a lacquer impervious to the solution. A part of this lacquer was then stripped off leaving an area of 0.5 cm^2 of bare metal exposed to the environment. A potentiostat curve for the no stress condition was obtained. The open area was remasked and another open area of the same size made prior to running the potentiostat curve for the stressed condition.

Potentiostat curves were obtained with a Wenking Potentiostat Model 61-TR. The experimental arrangement is shown schematically in Figure 35. All potentials reported are with respect to a saturated calomel electrode. Oxygenation was accomplished by bubbling through the solution during test, and deoxygenation by bubbling nitrogen. The stirrer was located 0.2 cm from the surface being measured. The solution was 3% NaCl, pH 6.5.

The measurements were made by applying a given potential (usually starting at -1400 mv but on occasion up to -2000 mv), and measuring the current after stabilization (usually about one minute). Successive values of potential were measured from negative toward positive to prevent formation of an anodic film. The results are presented in Figures 36, 37, 38, and 39.

The effect of oxygen was to shift the cathodic polarization curves in an electropositive direction. The Tafel slope, b_c, for Ti-5Al-2.5Sn was 0.07 V which agrees with Stern and Wissenberg's[31] value for the hydrogen reaction of titanium in hydrogen saturated 20% H_2SO_4. Assuming the transfer coefficient $\alpha = 1/2$, and since $b = 0.059/\alpha n$, then $n = 1.64 \cong 2$. This would indicate that one of the cathodic reactions in 3% NaCl is $2e + 2H^+ \rightarrow 2H$.

The large increase in current density with oxygenation indicates the strong depolarization effect due to oxygen. Thus it is apparent that cathodic reduction of oxygen $O_2 + 4e \rightarrow 2H_2O$ also contributes to the cathodic
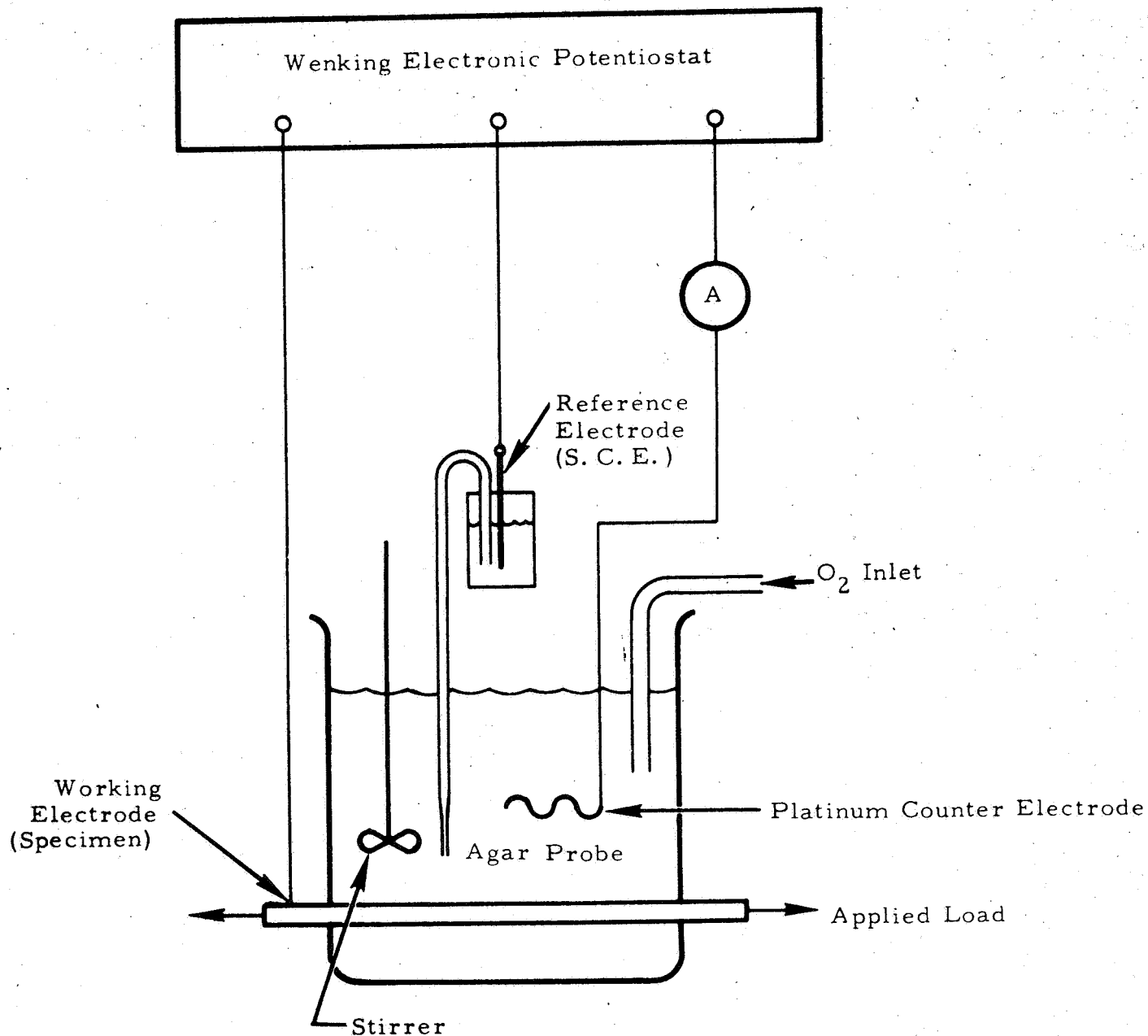
Figure 35. Schematic of Potentiostatic Experimental Arrangement
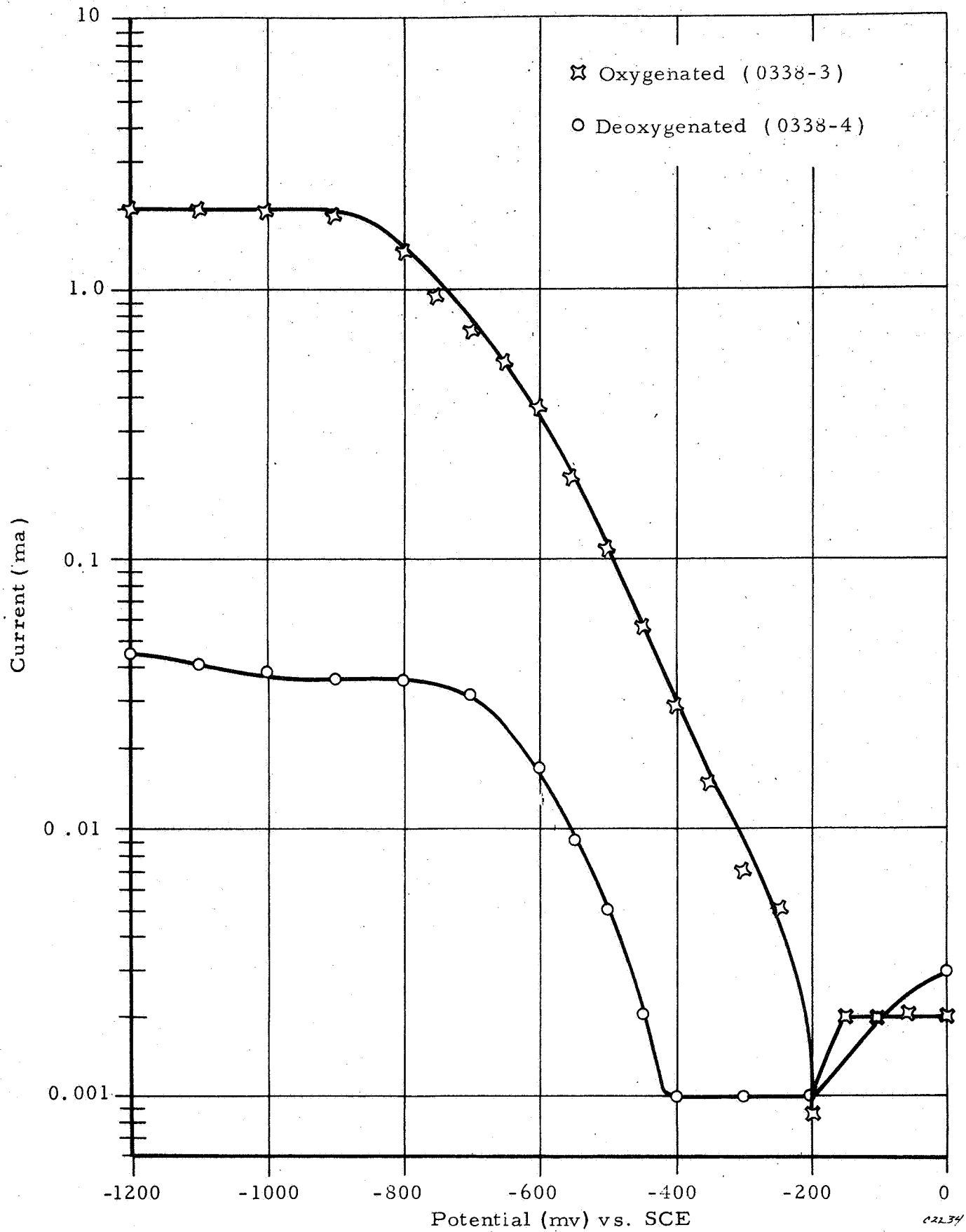
Figure 36. Effect of Oxygenation on the Polarization Curves of Ti-5Al-2.5Sn in 3% NaCl
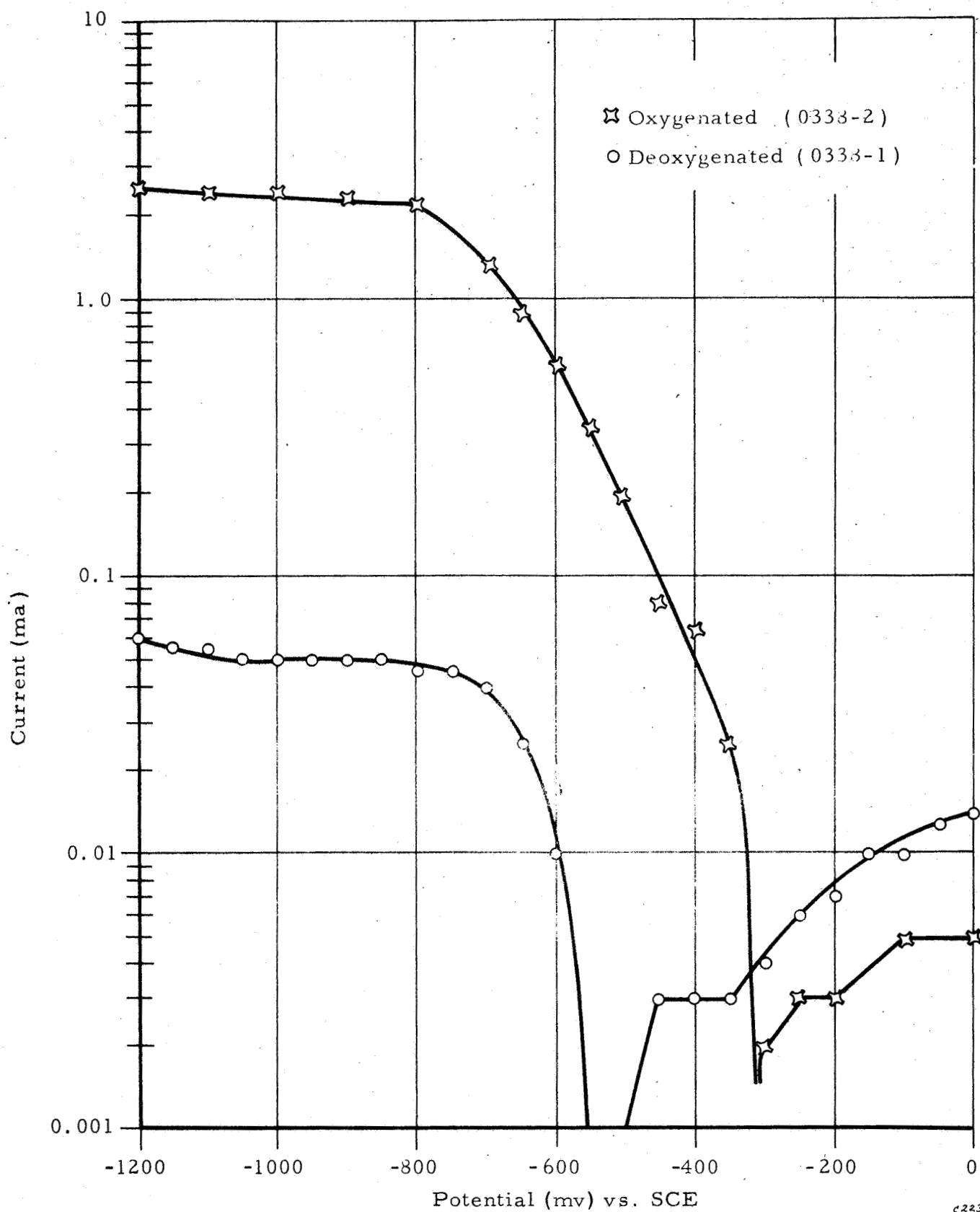
Figure 37. Effect of Oxygenation on the Polarization Curves
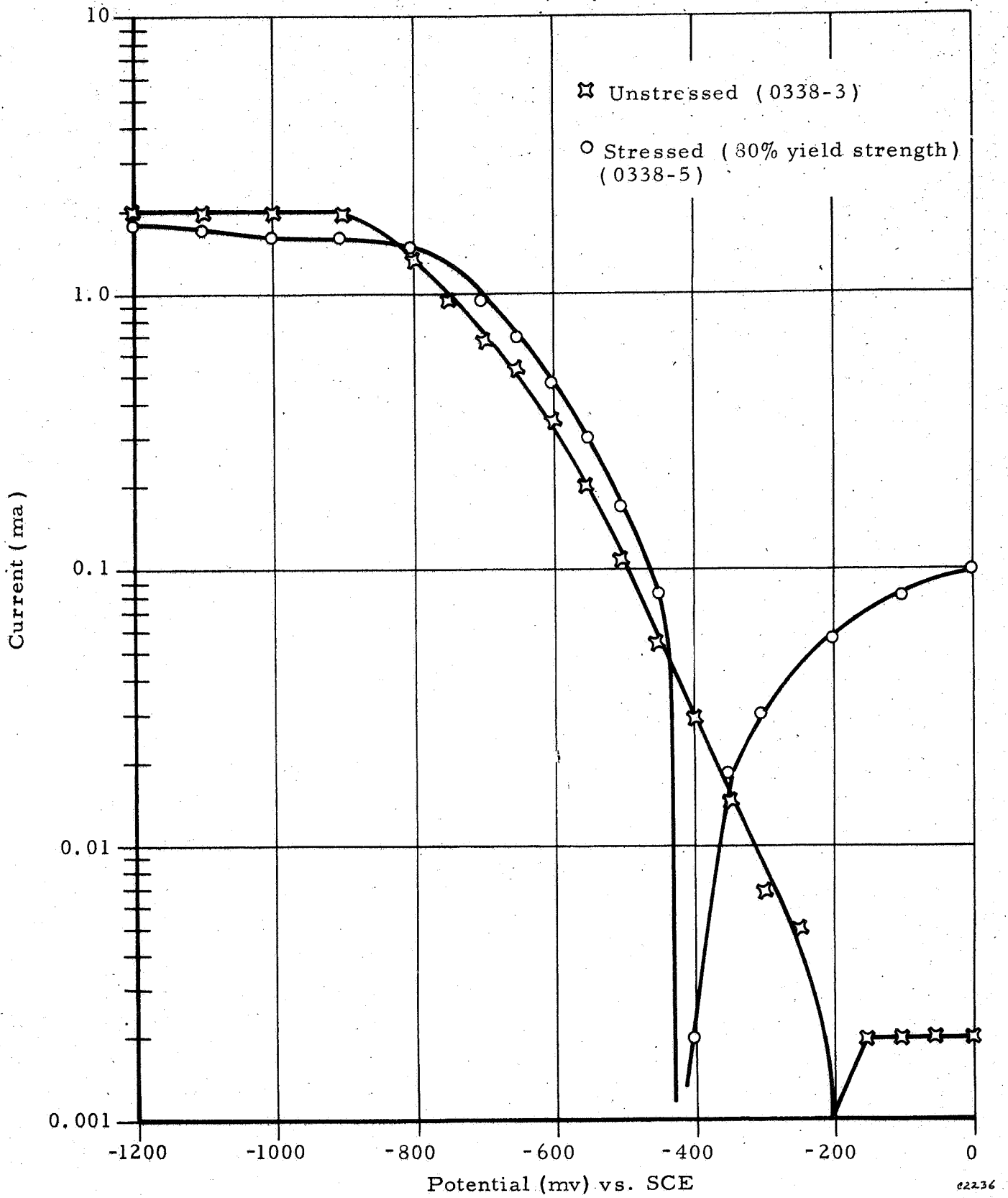of Ti-6Al-4V in 3% NaCl

Figure 38.   Effect of Stress on the Polarization Curve of
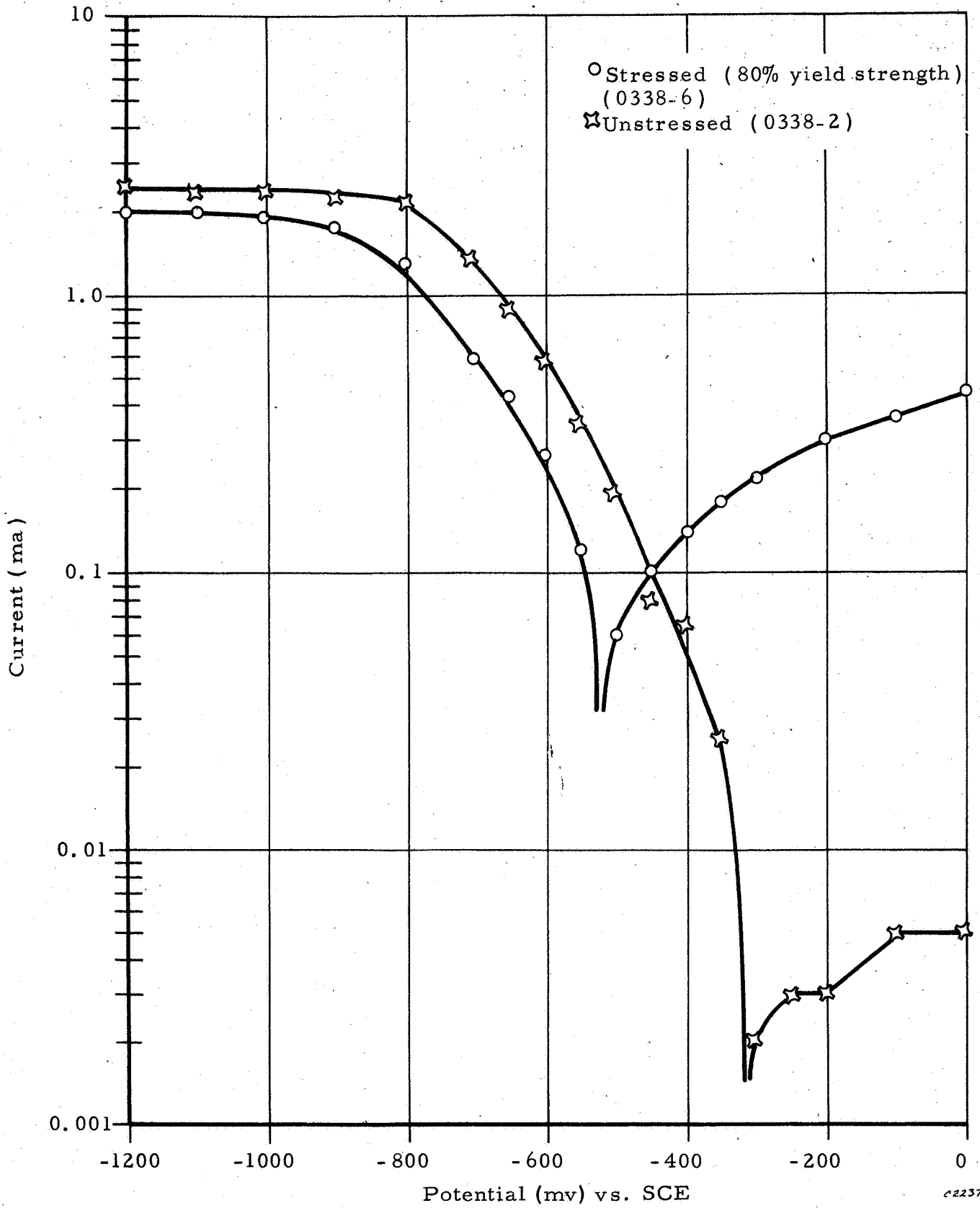Ti-5Al-2.5 Sn in 3% NaCl

Figure 39. Effect of Stress on the Polarization Curve of Ti-6Al-4V in 3% NaCl

polarization curve. Bubbling air through the solution produced the same results as did oxygen. Oxygenation did not greatly affect the anodic potential.

Stressing the specimens up to 80% of the yield strength did not greatly affect the cathodic polarization. The anodic branch, however, was greatly affected. Stress apparently reduced anodic passivation for both alloys. Thus the current at a given anodic potential was increased when stress was present.

To elucidate the effect of the hydrogen content of titanium alloys on the electrochemical behavior, polarization experiments were conducted with the alpha type alloy, Ti-5Al-2.5Sn, in oxygenated 3% NaCl solution at pH 6.5. Two types of alloy specimens were employed: (1) as received with 61 ppm hydrogen, and (2) vacuum annealed (10^{-6} torr) at 1400°F for 24 hours with 39 ppm hydrogen.

An examination of the polarization curves (Figures 40 and 41) indicated the following:

1. The rest potential of the alloy in unstressed condition was shifted in the electropositive (noble) direction with increased hydrogen content (from -0.4 V for 39 ppm, to -0.2 V for 61 ppm), and the anodic branch in the passive region was reduced in width.

2. Stressing to 80% of yield stress did not change the polarization curve in the passive region of the alloy with low hydrogen, but lowered the corrosion current (from about 0.02 to 0.003 ma/cm^2) in the passive region of the alloy with high hydrogen. Cathodic polarization branches were essentially the same. The anodic polarization branches in the transpassive region differed greatly, with the hydrogen content suggesting other complicated side reactions.

Alloying elements can alter corrosion behavior by affecting the polarization of either the anodic or cathodic reactions. If the alloying element assists the formation of a stable oxide on the anodic surfaces, passivation can result. However, the electrode polarization curves obtained in this study and those of Beck[26] show that composition has little effect on the basic corrosion reactions for titanium alloys in aqueous solutions containing alkali halides. The compositional dependence of the stress-corrosion behavior of titanium alloys appears to be related to the distribution of sites for localized attack.
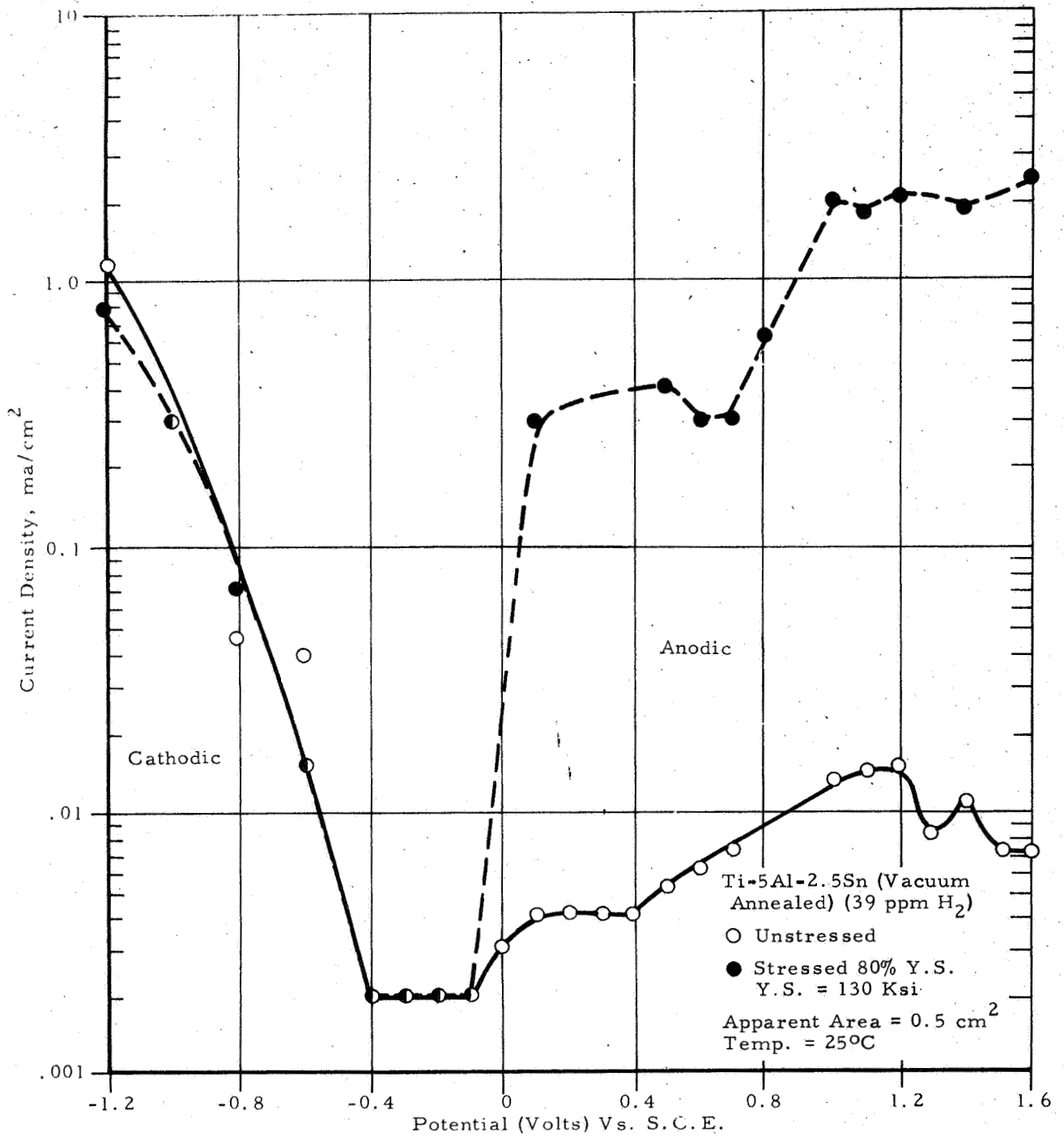
Figure 40. Polarization Curves of Vacuum Annealed Ti-5Al-2.5Sn
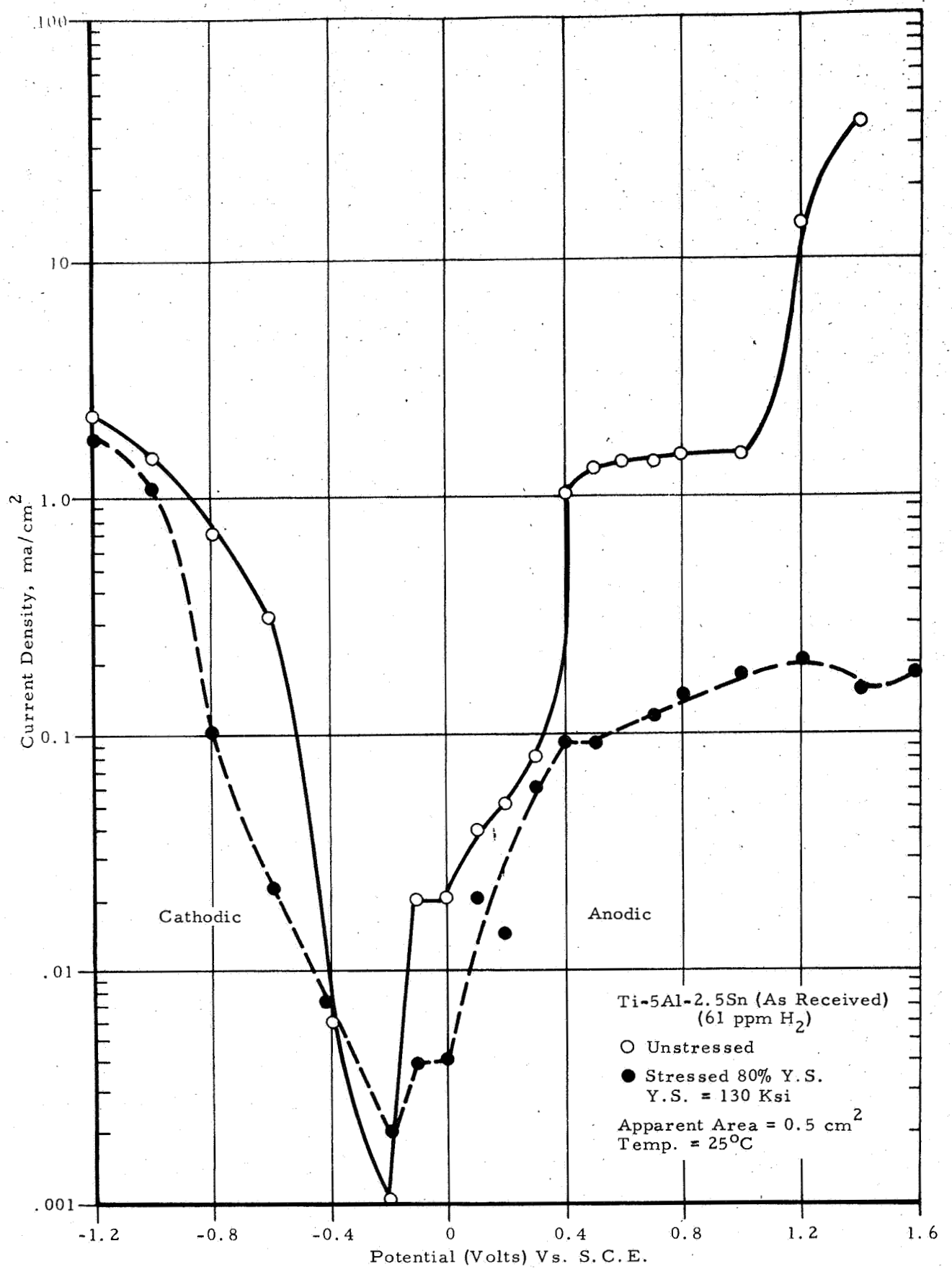Alloy in Oxygenated 3% NaCl, pH 6.5

Figure 41. Polarization Curves of Ti-5Al-2.5Sn Alloy
in Oxygenated 3% NaCl, pH 6.5

3.0   CONCLUSIONS

The results obtained from the current investigation, and the conclusions reached, are summarized below.

1. Precracked notched alpha type Ti-5Al-2.5Sn and alpha-beta type Ti-8Al-1Mo-1V alloys exhibited high sensitivity to crack propagation in distilled water and 3% NaCl solutions, whereas alpha-beta type Ti-6Al-4V and Ti-13V-11Cr-3Al were less sensitive in 3% NaCl solution, and did not exhibit noticeable effect in distilled water.

2. All beta alloys exhibit ductile dimple microstructure in fracturing in air and salt solutions. Alpha-beta type alloys exhibit mixtures of ductile dimple and brittle cleavage areas in fracture faces. The cleavage areas are much larger in stress cracking in aqueous salt solutions, compared to distilled water fracturing. The stress corrosion crack paths propagate transgranularly through alpha grains, but appear to follow by cleavage at the alpha-beta phase boundaries.

3. Electron microautoradiography studies clearly demonstrated that hydrogen gas in quantities less than 50 ppm (in radiotracer form H^3) introduced into titanium alloys is preferentially segregated in beta phase in alpha-beta type alloys, and is uniformly dispersed in all beta type alloys. The concentration of hydrogen in the beta phase of alpha-beta alloys containing approximately 40 ppm was estimated to vary from 285 ppm for Ti-6Al-4V, and approximately 450 for Ti-8Al-1Mo-1V and Ti-5Al-2.5Sn alloys. These high segregations of hydrogen in the beta phase appear to play a role in the brittle behavior of the beta phase and alpha-beta boundary regions.

4. High stress concentration around crack tips does not appear to cause hydrogen segregation or change in hydrogen distribution between the alpha phase matrix and beta phase particles in alpha-beta alloys.

5. Potentiostat curves were obtained for Ti-6Al-4V and Ti-5Al-2.5Sn in 3% NaCl with pH 6.5 in oxygenated and deoxygenated solutions in the unstressed and stressed to 80% of yield condition. The effect of oxygen was to shift the cathodic polarization curves in an electropositive direction. Thus it is apparent that cathodic reduction of oxygen $O_2 + H^+ + e \rightarrow 2 H_2O$ also contributes to the

cathodic polarization curves. Stressing the specimen up to 80% of yield did not greatly affect the cathodic polarization. Some electrochemical changes occur in the anodic branch and appear to be dependent on the hydrogen content of the material. The compositional dependence of the stress-corrosion behavior of titanium alloys appears to be related to the distribution of sites for localized attack.

6. It is shown that the preferential distribution of hydrogen in the beta phase appears to contribute greatly to the susceptibility of the alpha-beta (Ti-8Al-1Mo-1V) and near-alpha (Ti-5Al-2.5Sn) titanium alloys to stress corrosion cracking. Further studies are needed to elucidate the effect of different total hydrogen content on SCC, and also the change in hydrogen segregation by various solution treatments, or aluminum content and subsequent effect on the susceptibility to SCC.

REFERENCES

1. C. H. Avery and R. V. Turley, <u>Chloride Stress Corrosion Susceptibility of High Strength Steel, Titanium Alloy and Superalloy Sheet</u>, Air Force Mat. Lab., Tech. Doc. Rep. ML-TDR-64-44, Vol. 1, March 1964 and Vol. II, May 1964.

2. R. L. Kirchner and E. J. Ripling, "Elevated Temperature Stress Corrosion of High Strength Sheet Materials in the Presence of Stress Concentrations," First Interim Report on NASA, Contract NAS r-50, November 1964.

3. D. H. Braski and G. J. Heimerl, "The Relative Susceptibility of Four Commerical Titanium Alloys to Salt Stress Corrosion at 550°F," NASA TND-2011, December 1963.

4. B. F. Brown and C. D. Beachem, "A Study of the Stress Factor in Corrosion Cracking by Use of the Pre-cracked Cantilever Beam Specimen," <u>Corrosion Science</u>, 5 (1965), p. 745.

5. T. J. Lennox, Jr., editor, "Stress Corrosion Cracking of Titanium Alloys in Salt Water, Distilled Water and Sea Water," Marine Corrosion Studies, Third Interim Report of Progress, NRL Memorandum Report 1634, July 1965.

6. R. W. Judy, Jr., T. W. Crooke, R. E. Morey, E. A. Lange, and R. J. Goode, "Low-Cycle Fatigue-Crack Propagation and Fractographic Investigations of Ti-7Al-2Cb-1Ta and Ti-6Al-4V in Air and in Aqueous Environments," <u>Trans. ASM</u>, 59 (1966), p. 195.

7. Reactive Metals, Inc., "Preliminary Data on the Aqueous Stress Corrosion Cracking of Titanium Alloys," September 28, 1965.

8. I. R. Lane, Jr., O. L. Cavallaro, and A. G. S. Morton, <u>Fracture Behavior of Titanium in the Marine Environment</u>, U. S. Navy MEL Report 231/65, July 1965.

9. A. J. Hatch, H. W. Rosenberg, and E. F. Erbin, "Effects of Environment on Cracking in Titanium Alloys," presented to ASTM Pacific Area National Meeting, Seattle, Washington, November 1965.

10. T. R. Beck, <u>Stress Corrosion Cracking of Titanium Alloys, Heat Treatment Effects, Stress Corrosion Cracking in Various Solvents and Electrochemical Kinetics with Ti-8Al-1Mo-1V Alloy</u>, Contract NAS 7-489, Progress Report No. 2, December 1966.

11. G. F. Erbin, "Recent Developments in the Processing of Titanium," a paper presented at the AIME Annual Meeting, Los Angeles, February 1967.

12. T. J. Murphy and N. G. Feige, "Preliminary Evaluation of Degradation of Titanium Crack Resistance in Sea Water Environment," Titanium Metals Corp. of America, May 7, 1965.

13. T. L. Mackay and C. B. Gilpin, Stress Corrosion Cracking of Titanium Alloys at Ambient Temperature in Aqueous Solutions, Report SM-49105-Q2, NAS 7-488, January 1967.

14. T. J. Murphy and N. J. Feige, "Fracture Behavior of Titanium Alloys in Aqueous Environments," presented to WESTEC, Los Angeles, March 1966.

15. F. A. McClintock and G. R. Irwin, "Plasticity Aspects of Fracture Mechanics," ASTM-STP 381, April 1965.

16. W. F. Payne, "Incorporation of Fracture Information in Specifications," AD 621-840, Edwards AFB, 1964.

17. W. F. Brown, Jr. and J. E. Strawley, "Plane Strain Crack Toughness Testing of High Strength Metallic Materials," ASTM STP 410, 1967.

18. M. F. Amateau and E. A Steigerwald, "Fracture Characteristics of Structural Metals," ER-5937-3, Thompson-Ramo-Woolridge, Inc., Cleveland, Ohio, June 1965.

19. J. E. Strawley and W. F. Brown, Jr., "Fracture Toughness Testing Methods," ASTM STP 381, April 1965.

20. B. F. Brown and C. D. Beachem, Corrosion Science, 5 (1965), p. 745.

21. A. Phillips, V. Kerlins, and B. V. Whiteson, Electron Fractography Handbook, ML-TDR-64-416 AFML-Wright Patterson AFB, January 1965.

22. L. W. Berger, D. N. Williams, and R. I. Jaffee, Trans. AIME, 212 (1958), p. 509.

23. O. J. Huber, J. E. Gates, A. P. Young, M. Pobereskin, and P. O. Frost, Trans. AIME, July 1957, p. 918.

24. R. J. Quigg and A. R. Troiano, "Hydrogen Embrittlement and Strain Aging in Titanium Alloys," WADC-TR-59-172, April 1959.

25. R. I. Jaffee and D. N. Williams, Trans. Am. Soc. Metals, 51 (1959), p. 820.

26. T. R. Beck, "Stress Corrosion of Titanium Alloys, Preliminary Report on Ti-8Al-1Mo-1V Alloy and Proposed Electrochemical Mechanism," Boeing Document D1-82-0554 (July 1966).

APPENDIX A

MICROAUTORADIOGRAPHIC RECORDING EFFICIENCY FOR BETA-ACTIVITY IN TRITIATED TITANIUM

Prepared by S. K. Asunmaa

APPENDIX A

MICROAUTORADIOGRAPHIC RECORDING EFFICIENCY FOR BETA-ACTIVITY IN TRITIATED TITANIUM

An emulsion efficiency may be defined as the ratio of the number of filaments observed in the electron microautoradiograph per square centimeter to the number of beta particles reaching the emulsion.

For the titanium experiments two of the alloys, Ti-5Al-2.5Sn and Ti-13V-11Cr-3Al, exhibited fairly uniform distribution. The alloy Ti-5Al-2.5Sn was used to calculate emulsion efficiency, since the heavier elements V and Cr will probably absorb more beta. The estimated filament density for this alloy was 19.3×10^8 filaments per square centimeter.

In order to calculate the number of beta particles reaching the emulsion, the volume of metal containing the radioactive element tritium which contributes to the emulsion exposure must be determined. The disintegrations per square centimeter during exposure must be estimated and corrected for the self-absorption of beta particles in titanium and for the geometry of exposure.

In general, nuclear electrons emitted in a single beta decay mode have a continuous energy distribution with a maximum energy (E) characteristic for transition element.[A1] For tritium, (E) is 0.018 MeV. The absorption curves of nuclear electrons start exponentially, and the intensity drops with a factor of two for every added (initial) half-thickness ($d_{1/2}$) related to the range (R) by $d_{1/2} = 0.1R$. The range-energy relation for aluminum is shown in Figure A-1.[A2] The half thickness for absorbers other than aluminum, such as titanium, can be evaluated using the empirical expression of Fournier[A3]

$$d_{1/2}(Ti) = d_{1/2}(Al) \times \frac{118}{105+22} = d_{1/2}(Al) \frac{118}{127}$$

The maximum range for H^3-beta penetration in titanium thus approximates 0.60 mg/cm^2.

A graphic presentation of the half-thickness-range dependency is used as a basis for evaluation of the total transmitted intensity. The transmitted intensity is a logrithmic function of half-thickness and may be expressed by the power equation
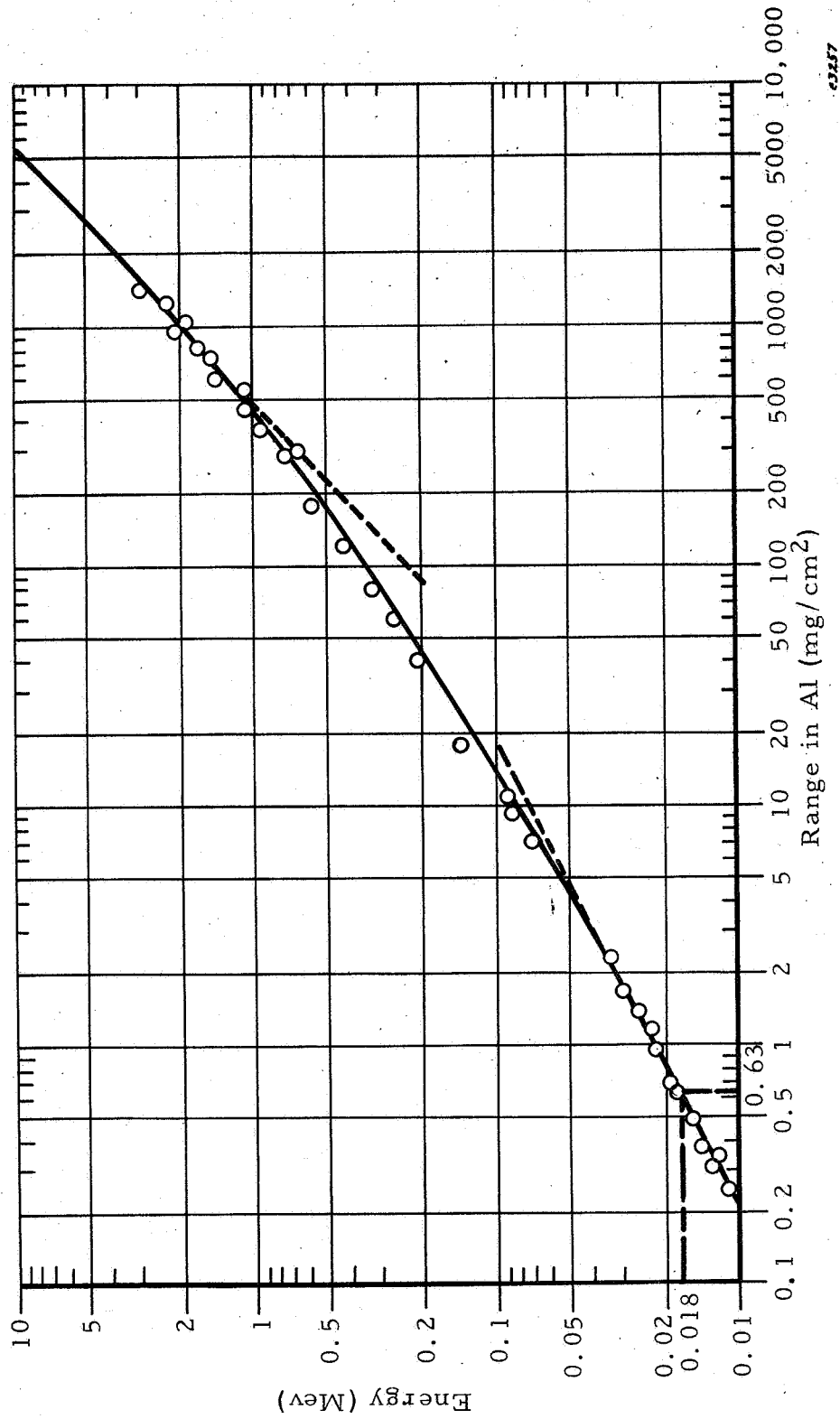
Figure A-1. Empirical Range Energy Relationship for Monoenergetic Electrons Absorbed in Aluminum According to Data From Schonland, Varder, Madgwick, Marshall and Ward, and Katz and Penfold. For nuclear electrons the range co-ordinate indicates the maximum range R_m. The H^3-beta R_m in aluminum is 0.63 mg/cm^2 (Reference 2).

$$I = I_o \left(\frac{1}{2}\right)^n$$

$$n = \text{number of half thicknesses}$$

The graphic presentation of the function is given in Figure A-2. The graph is constructed so that the initial number of the incident electrons decreases by a factor of two for each $d_{1/2}(Ti, H^3)$. The function may be integrated between $n = o$ and $n = m$ (number of half thicknesses for a significant range R_S) to determine the fraction (F_1) of the total incident electron beam intensity transmitted after self absorption

$$F_1 = \sum_{n=o}^{n=m} \left(\frac{1}{2}\right)^n dn$$

The detailed computation is given in Table A-I. On the basis of graphic integration from Figure A-2, it will be seen that a tritiated titanium layer, 0.01 mg/cm^2 thick, in a depth of 4 half thicknesses (0.08 mg/cm^2) contributes only 7% of its total radiation to the emulsion recording. The fraction of the total beta radiation intensity transmitted through titanium at this 0.08 mg/cm^2 thickness is

$$\frac{58.6}{20 \times 8} = 36\%$$

The error introduced by neglecting the contribution of the beta radiation from the depths greater than this thickness is calculated to be 5%, or less than the experimental error in filament density determination from microautoradiographs.

The tritium atoms emitting beta particles are evenly distributed in a surface layer of thickness, $R = 0.08$ mg/cm^2. For Ti-5Al-2.5 with density of 4.46 g/cm^3, this equals to 1.8×10^{-5} cm. Beta particles from tritium atoms can be emitted in any possible direction. Not all the beta particles emitted reach the emulsion, but only those emitted in the cone with the angle varying between $\pi/2$ and zero when the distance of beta particle source to the emulsion varies from $a=0$ to $a=R_S(\varphi=0)$ (see Figure A-3). The fraction of beta rays (emitted from P in an arbitrary direction) reaching the recording plane (CKC') is determined by the ratio of the spherical segment area to that of a sphere with radius $R_S(\varphi=0)$
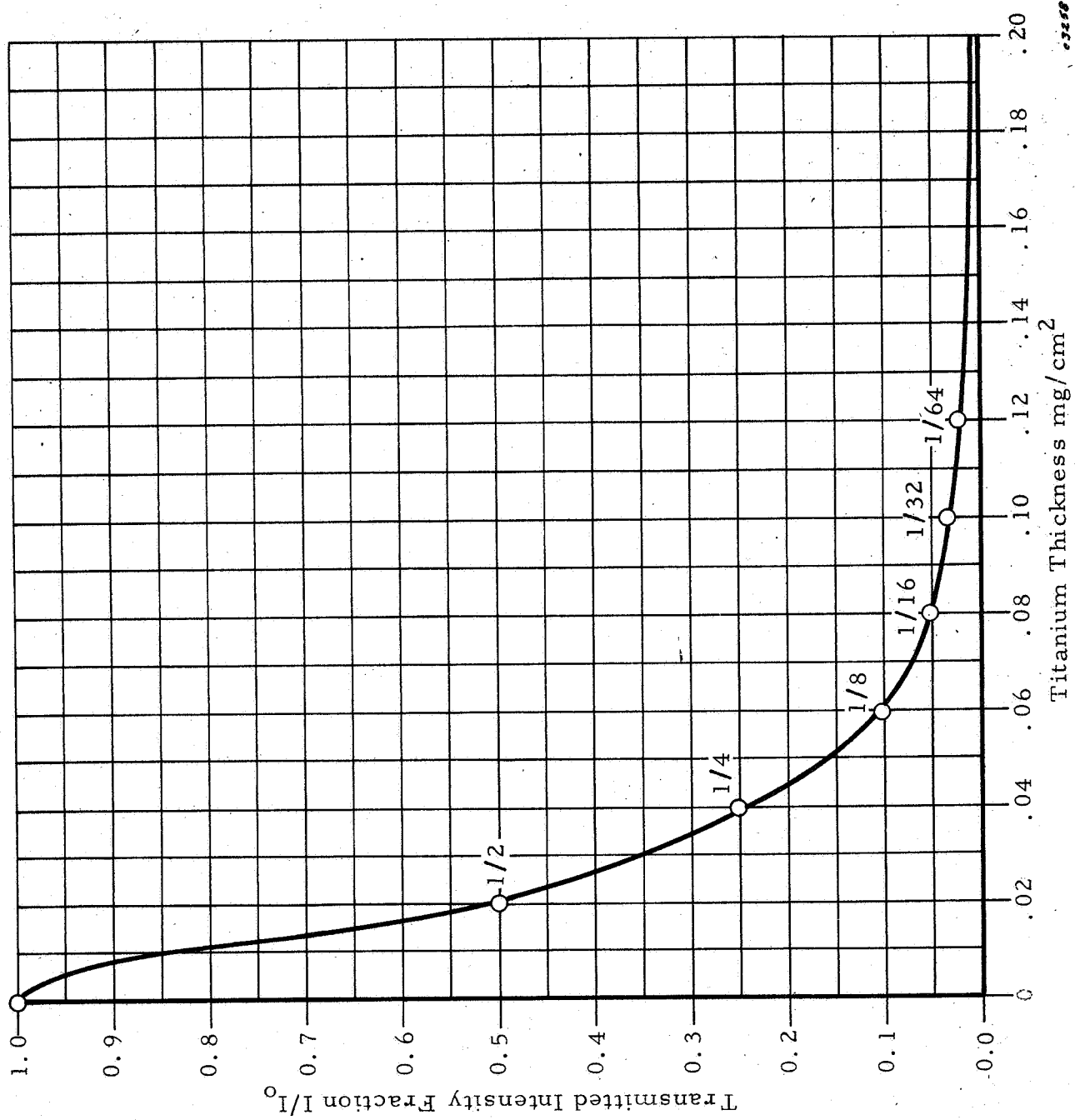
Figure A-2. Transmitted Tritium Beta (Energy Intensity Fraction Versus Titanium Mass Thickness)

TABLE A-I

NUMERICAL DATA FOR DIAGRAM IN FIGURE A-2

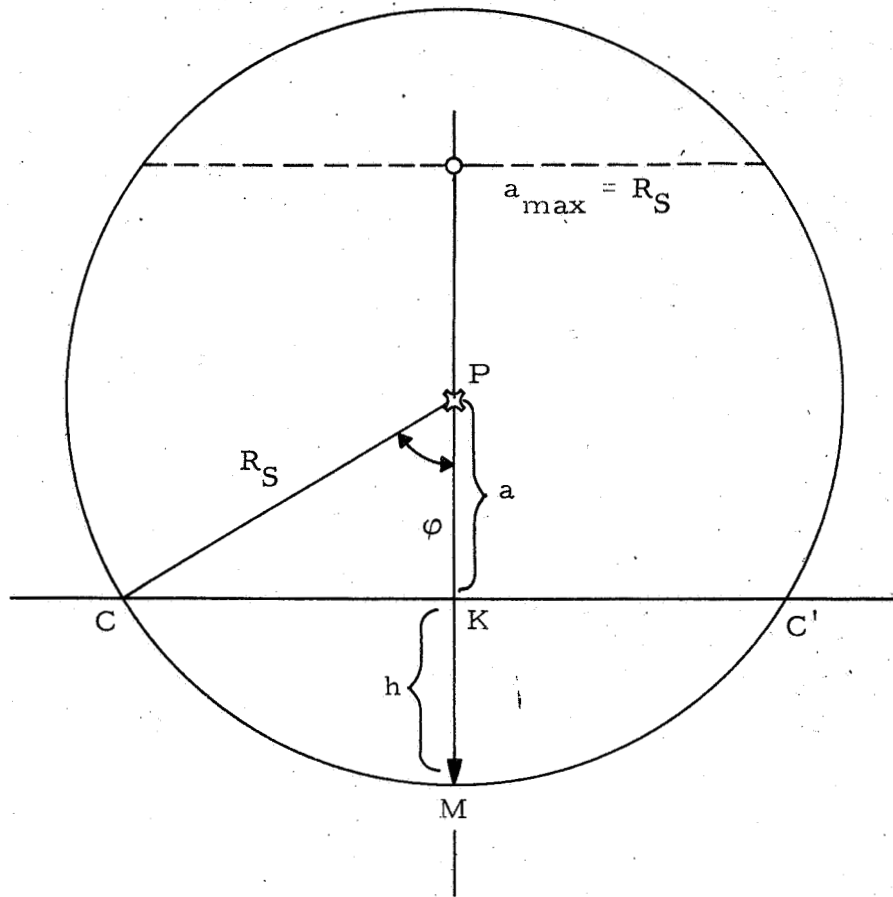| No. of Half Thickness (n)	Thickness mg/cm^2	$\dfrac{I}{I_0}$	Graph Area At Specimen Thickness	$\displaystyle\sum_o^n \dfrac{I}{I_0}$ In 20 Units Per $\frac{1}{2}d_{1/2}$
	0.01		97.5	19.5
1	0.02	1/2	70.0	33.5
	0.03		42.5	42.0
2	0.04	1/4	30.0	48.0
	0.05		21.0	52.2
3	0.06	1/8	15.0	55.2
	0.07		10.0	57.2
4	0.08	1/16	7.0	58.6
	0.09		5.0	59.6
5	0.10	1/32	4.0	60.4
	0.11		2.5	60.9
6	0.12	1/64	2.0	61.3
	0.13		1.5	61.6
7	0.14	1/128	1.0	61.8

Figure A-3. Spatial Distribution of Disintegration Signals
From a Point Source P at a Distance (a) From
the Emulsion Surface CKC'.

$$\frac{\text{area of spherical segment}}{\text{area of sphere}} = \frac{2\pi R_S^2 (1-\cos\varphi)}{4\pi R_S^2} = \frac{1-\cos\varphi}{2}$$

The total fraction (F_2) of electrons transmitted along the exposure geometry consideration can be calculated by varying the distance (a) of the point source to the emulsion surface from a=0 (for $\varphi = \pi/2$) to a=R_S (φ=0). The graphical computation of the data gives

$$F_2 = 36.4\%$$

The total fraction of beta radiation reaching the emulsion surface will be the fraction being transmitted after self absorption multiplied by fraction obtained from geometry distribution considerations

$$F = 0.36 \times 0.364 = 0.131$$

The volume of the alloy contributing to each square cm of emulsion is $1.8 \times 10^{-5} \times 1$ cm^2. The total number of tritium (H^3) atoms present in this volume which contains 48 ppm carrier free tritium by weight is

$$N = \frac{1.8 \times 10^{-5} \times 4.46}{3} \times 48 \times 10^{-6} \times 6.02 \times 10^{23} = 7.68 \times 10^{14}$$

The number beta particles or disintegrations from the long half-life tritium nuclei can be calculated from the expression

$$N_o - N = N_o \lambda t$$

t = disintegration or exposure time, 16 hours

λ = disintegration constant $\dfrac{0.643}{t_{1/2}} = 6.3 \times 10^{-6}$ hrs^{-1} = 1.82×10^{-9} sec^{-1}

$N_o - N = 7.68 \times 10^{14} \times 1.82 \times 10^{-9} \times 16 \times 3600$

$\qquad = 8.05 \times 10^{10}$

The amount of beta particles reaching the emulsion surface is therefore

$$8.05 \times 10^{10} \times 0.131 = 1.05 \times 10^{10}$$

The emulsion efficiency estimated from Ti-5Al-2.5Sn microautoradiographs is therefore

$$\frac{\text{filaments/cm}^2 \text{ observed}}{\text{beta particles reaching surface}} = \frac{19.3 \times 10^8 \times 100}{1.05 \times 10^{10}} = 18\%$$

REFERENCES

A1.   A. H Wapstra, G. J. Nijgh, and R. VanLieshaut, <u>Nuclear Spectroscopy Tables</u>, North Holland Publishing Co., Amsterdam, 1959, p. 40.

A2.   R. D. Evans, <u>The Atomic Nucleus</u>, McGraw-Hill Book Co., Inc., New York, 1955 (International Series in Pure and Applied Physics).

A3.   G. Fournier, <u>Ann. Phys.</u>, 8, 206 (1927), Paris.